DEPLETION OF TDP-43 ACCELERATES NEURODEGENERATION IN AN ALZHEIMER'S MOUSE MODEL, INDEPENDENT OF BETA-AMYLOID PLAQUE BURDEN

By
Katherine D. LaClair

A dissertation submitted to Johns Hopkins University in conformity with the requirements for the degree of Doctor of Philosophy

Baltimore, Maryland
June, 2016

ABSTRACT

TDP-43 proteinopathy, initially associated with ALS and FTD, is also found in 30-60% of Alzheimer's disease (AD) cases and correlates with worsened cognition and neurodegeneration. A major component of this proteinopathy is depletion of this RNA-binding protein from the nucleus, which compromises repression of nonconserved cryptic exons in neurodegenerative diseases. To test whether nuclear depletion of TDP-43 may contribute to the pathogenesis of AD in cases with TDP-43 proteinopathy, we examined the impact of depletion of TDP-43 in populations of neurons thought to be vulnerable in AD, and on neurodegeneration in an AD-linked context. Here, we show that TDP-43 depletion in forebrain neurons accelerates neurodegeneration in an AD mouse model independent of the Aβ plaque burden. Moreover, populations of large pyramidal neurons in the forebrain that are selectively vulnerable in AD are also vulnerable to TDP-43 depletion. These findings support a role for nuclear depletion of TDP-43 in the pathogenesis of AD and provide strong rationale for developing novel therapeutics to alleviate the depletion of TDP-43, creating functional ante-mortem biomarkers for early detection, and stratifying AD subjects with TDP-43 pathology to empower clinical trials.

PREFACE

Acknowledgments

This work was supported in part by the JHUSOM Neuropathology Frederick J. Pelda Alzheimer's Research Fund, the Robert Packard Center for ALS Research, the Amyotrophic Lateral Sclerosis Association and NIH grant R01-NS095969. The authors wish to thank Venette Nehus and Barbara Smith for technical assistance.

Dedication

To Paul L. LaClair and Debra LaClair, whose love and support have allowed me to discover my fullest capabilities. And to Matthew LaClair, who taught me about bravery and the importance of being true to myself.

TABLE OF CONTENTS

LIST OF TABLES

LIST OF FIGURES

INTRODUCTION

Alzheimer's disease

Alzheimer's disease (AD) is the most common cause of dementia[1] and the fifth leading cause of death among the elderly in the United States[2]. Dementia is a debilitating condition characterized by a progressive loss of cognitive function, behavioral changes, and a decline in performing activities of daily living[3]. In AD, these deficits are caused by a loss of synapses, and eventually neurons, beginning in the hippocampus and forebrain[4], areas critical for memory, and executive functions like planning and making decisions. Eventually, as neurodegeneration spreads to other parts of the brain, patients lose the ability to perform basic movements like walking, talking, swallowing, and even breathing. The severity of these deficits and the slow progression of the disease mean that many AD patients reliant on constant, attentive care for many years, leading to direct and indirect health care costs of over $450 billion in 2015[5]. These costs continue to rise as more people live longer and effective disease-modifying treatments remain unavailable.

Though AD patients typically display noticeable cognitive symptoms in the 6th or 7th decade of life, there is evidence that neuronal dysfunction and degeneration begin several decades earlier[6,7]. Therefore, once cognitive decline becomes apparent, many synapses and neurons have already been lost, and this physical damage is likely irreversible. This suggests that understanding the pathogenesis of AD before permanent neuronal damage takes place may accelerate the development of effective therapeutics. Significant improvements in the development of biomarkers for use in living patients have made clinical trials in early and pre-symptomatic stages of AD feasible, potentially improving the chances for successful therapeutic intervention at early stages of the disease[8,9].

Canonical hypotheses of AD

The first major hypothesis of AD pathogenesis was the "amyloid cascade hypothesis" formalized by Hardy and Higgins in 1992[10]. It posits that extracellular Aβ deposits, called plaques, are the primary cause of AD and directly lead to tau neurofibrillary tangles, followed by synapse degeneration and cell loss in an essentially linear cascade manner. A strong role for Aβ in AD is supported by genetic linkage studies showing that mutations in genes responsible for Aβ production (*APP*, *PSEN1*) lead to inherited forms of AD with nearly complete penetrance[11]. In addition, *APOE*, which has been implicated in Aβ clearance[12,13], was identified as a strong modifier of AD risk[14,15]. Since the amyloid cascade hypothesis was formulated, a large body of evidence has accumulated indicating that some form(s) of soluble/diffusible, multimeric Aβ oligomers, rather than plaques *per se*, initiate AD neurodegeneration (reviewed in[16]). Therefore, the modern amyloid cascade hypothesis posits that Aβ oligomers are the causal factor in the cascade. This process now also includes dysfunctional synaptic plasticity and neuroinflammation as important contributors in the disease[16]. Intriguingly, compounds that disaggregate Aβ oligomers improve cognition and reduce glial inflammation in AD-linked mutant mice, even when administered after onset of plaque deposition and cognitive deficits[17], indicating that Aβ-induced damage may be reversible, particularly before the onset of tau pathology. Potentially promising Phase II results of a small Aβ immunization trial[18] have led to over a dozen antibody trials that are currently underway[19].

While strong evidence supports a linear progression of disease caused by Aβ in familial AD, the evidence in sporadic AD supports a more multifactorial etiology[8,9,20,21].

First, the risk genes associated with sporadic AD by genome-wide association studies are involved in immune function, lipid biology, and endocytosis[8]. While there is reasonable evidence that many risk genes, including APOE[13,22], CLU[23], SORL1[24], and ABCA7[25], regulate various facets of Aβ metabolism *in vivo*[26], additional functions have been demonstrated for many of these factors that could explain neurodegeneration independent of Aβ[27–29]. In addition, several of the AD risk genes are also implicated in neurodegenerative diseases with no Aβ pathology[28,30], which suggests that they do not promote dysfunctional Aβ dynamics. Instead, the diversity of function of AD risk genes further supports multiple pathogenic factors in sporadic AD. Interestingly, the strongest risk factor for AD is aging[5], and there is evidence that age-related stresses including oxidative stress[31,32], mitochondrial dysfunction[33] and inflammation[34] can induce pathogenic processing of Aβ. Head injury is another major risk factor for AD, particularly in individuals carrying the ApoE4 risk allele[35–37], and can lead to both Aβ deposition and tau tangle formation[26]. This "reactive" formation of AD pathology indicates that cases of dementia with Aβ and tau pathology can exist where Aβ is a byproduct or late contributor, rather than a major driver of disease. Importantly, Aβ-targeted therapies could be expected to have minimal or no effect on cognitive decline in these cases.

Many clinical findings also support multifactorial etiologies in sporadic AD. First, a large proportion (~30%) of clinically diagnosed AD cases do not meet the pathologic criteria for plaques and tangles at autopsy[38]. While a common explanation for this is that these are misdiagnosed cases of another dementia, others have noted that the assumption that all AD cases must have plaques and tangles may not be well-supported[20,21]. For

example, patients carrying the Osaka *E693Δ APP* mutation produce highly oligomeric Aβ that is resistant to proteolytic degradation, but does not form fibrils or plaques[39]. As a recent review cogently argues[21],

> "*... to list amyloid deposits as a required part of the definition of [AD] is supported neither by the data nor by the clinical experience. It is the equivalent of saying that once plaques are found in the coronary arteries, a person is having a heart attack and, if there are no plaques in the arteries, no myocardial event can be defined as a heart attack. This is not a useful concept. Rather, in both heart and brain, the plaques define risk, not disease.*"

Though plaques can be a useful visible indicator that damaging oligomeric Aβ is present at high levels in the brain, they do not correlate well with pathogenesis or cognitive decline[40,41]. As in the case of heart attack, the same clinical presentation of AD (or the same functional failure of a particular population of neurons) may arise in different individuals through multiple pathogenic mechanisms. Additionally, multiple independent etiologies have been well-demonstrated in cancers[42–44] which, like AD, have a high degree of complexity and have resisted treatment efforts.

The second clinical finding that supports multifactorial etiologies for AD is that 20-40% of cognitive normal individuals are nonetheless pathologically indistinguishable from those with severe clinical symptoms of AD[38,45]. This suggests that Aβ and tau pathologies are not sufficient to cause "the complex symptomatology of AD"[21], and that other pathogenic factors may contribute. Indeed, recent work showed that non-canonical pathologies occur in up to 75% of AD cases[46,47] including TDP-43 proteinopathy, α-

synuclein “Lewy bodies”, and tau “Pick bodies” that each contribute to neurodegeneration in separately classified diseases[48–50]. Together, these findings suggest that Aβ is one of many initiators of sporadic AD as part of a complex set of conditions that lead to cognitive failure[9,21].

TDP-43 as a non-canonical pathogenic factor in AD

Increasing evidence suggests that nuclear depletion of the transactivation response element DNA-binding protein 43 (TDP-43) may be a non-canonical pathogenic factor in AD. As noted previously, TDP-43 proteinopathy, characterized by nuclear depletion and cytoplasmic aggregation, is commonly found in neurodegenerative diseases[48] including AD[51]. Notably, TDP-43 proteinopathy is strongly associated with worsened cognition in AD cases[52]. TDP-43 is involved in translational repression[53], RNA metabolism[54,55], and splicing[56–58] that have been shown to impact neurofilament stability[59] and synaptic plasticity[53]. *Tdp-43* is an essential gene[60] that regulates a large number of pre-mRNAs[61] and its protein level is tightly controlled through auto-regulation[62]. Therefore, both increased[63] and decreased[60] expression of TDP-43 lead to early death, while animals with heterozygous knockout of *Tdp-43* maintain normal protein levels[60].

TDP-43 is known to migrate from the nucleus to the cytoplasm under conditions of stress[54,55], forming normally short-lived protein-RNA complexes called stress granules. Interestingly, other RNA binding proteins that take part in stress granule formation have been shown to be susceptible to fibrillization during this process[64,65], indicating one mechanism by which TDP-43 might be depleted from the nucleus in sporadic AD. These fibrils shares structural commonalities with Aβ and tau aggregates in AD, and also with α-synuclein aggregates in Parkinson’s, suggesting that a common age-

related cellular mechanism may lead to aberrant aggregation of proteins in many neurodegenerative diseases of aging[66,67].

Previously, we found that TDP-43 is a splicing repressor of nonconserved cryptic exons in multiple cell types, including neurons, and that this function is compromised in the neurodegenerative disease spectrum of amyotrophic lateral sclerosis and frontotemporal dementia (ALS-FTD)[68]. Specifically, nuclear depletion of TDP-43 leads to incorporation of nonconserved cryptic exons that often induce nonsense mediated decay of the associated mRNAs, potentially altering the proteome of TDP-43 depleted cells. Importantly, we recently found that TDP-43-associated cryptic exons are also incorporated in the brains of AD cases with TDP-43 pathology (Chen *et al*., unpublished), indicating that nuclear depletion of TDP-43 may indeed contribute to the pathogenesis of AD. In addition, current clinico-pathologic evidence indicates that TDP-43 proteinopathy occurs independent of Aβ; the presence of one pathology does not make the other more likely to occur[47]. This suggests that TDP-43 proteinopathy and Aβ pathology may mark the presence of separate pathogenic mechanisms that contribute independently to neurodegeneration. Specifically, we hypothesize that nuclear depletion of TDP-43 contributes to AD pathogenesis in cases with TDP-43 proteinopathy. The outcome of studies to test this hypothesis, whether positive or negative, could inform therapeutic development as well as the design and interpretation of clinical trials. For example, up to 75% of AD cases have TDP-43 dysfunction[52] that may require treatment separate from Aβ-related dysfunction. If they contribute equally to disease pathogenesis, clinical trials of Aβ-targeting therapies that do not exclude or stratify TDP-43-affected patients would have dramatically reduced power, and may fail even if the therapy is

effective against Aβ. Conversely, if depletion of TDP-43 does not contribute to AD pathogenesis, then continuing failures of current Aβ-directed clinical trials would further support the idea that the amyloid cascade hypothesis is not sufficient to explain AD pathogenesis. As this question has far-reaching consequences for therapeutic development, experimental models that can test these hypotheses are of great interest.

Modeling AD pathogenesis in mice

Mechanistic understanding of AD pathogenesis is crucial for the efficient development of therapeutic strategies. Genetically modified mice allow researchers to study various facets of AD in an intact mammalian system, and over 100 such models have been developed to date (alzforum.org/research-models). Genetically modified mice are particularly well-suited for studying gene function and the contributions of broad cell types (neurons, microglia, etc.) to disease pathogenesis. Most AD models contain alterations in one or more AD-linked genes that encode or process aggregative proteins characteristic of the disease; *APP* (50%), *PSEN1* (23%), *MAPT* (tau) (19%), and *ApoE* (8%) (www.alzforum.org/research-models). Of these, 29 models overexpress or knock-in mutant human APP. Though many of these models develop plaques with regional specificity that is very similar to human AD[69–79], plaque formation is not necessary to produce cognitive deficits[80–82]. In addition, though these models generally exhibit very mild, if any, neuron loss[70,81], there is evidence of synaptic degeneration and plasticity impairments[75,83].

One of the most commonly used mouse models, developed by Dr. David Borchelt and co-workers, is the *APP_{swe}/PS1ΔE9* line, carrying two AD-linked mutations (*APP K595N/M596L* and *PSEN1* deletion of exon 9) in a humanized APP sequence expressed

under the control of the mouse prion promoter[84]. These mutations lead to an increased Aβ42/40 ratio in the brain[84,85], and visible Aβ plaques begin to develop around 4 months of age[85]. In addition, these mice display several other phenotypes characteristic of AD, including neuritic and synaptic degeneration[86–88], neuroinflammation[87,89], mitochondrial dysfunction[90], and cognitive deficits[89,91]. Interestingly, several studies have reported the ability of various Aβ-targeting interventions to reverse degenerative phenotypes, usually back to wild-type levels, even after extensive physical damage has taken place[17,92]. However, whether these degenerative phenotypes are also reversible in the human disease remains unclear, and current Aβ-targeting trials in humans should provide further data to address this question. Importantly, increased tau phosphorylation also occurs in these mice[89,90], though frank tangles (a structurally-defined form detected using the Gallyas silver stain[93]) do not form. This lack of tangles is a common finding among AD-linked mutant mice[94], and has raised further concerns about the accuracy of the amyloid cascade hypothesis and its proposition that Aβ directly stimulates the formation of tau tangles.

To further explore the relationship between Aβ and tau, additional models co-expressing AD-linked mutations and human tau were developed. Disappointingly, mice overexpressing wild-type human tau did not form tangles, and the phospho-tau aggregates that did form did not require AD-linked mutations[95]. However, these experiments did indicate that Aβ was capable of initiating the hyper-phosphorylation of tau that presumably is a precursor to its conformational shift into tangles. Shortly after, the LaFerla group developed the 3xTg mouse model expressing mutated *P301L* 4-repeat tau linked to frontotemporal dementia (FTD)[96] along with two AD-linked mutations. Pathologically, these mice mimicked AD, with plaque formation preceding tau tangles[97].

However, the relevance of this model to AD is disputed since tau *P301L* can form tangles in the absence of AD-linked mutations, and this mutation causes FTD, not AD, in humans[98].

Since that time, our group has shown that expressing the 4-repeat fragment of wild-type human tau in *APP_{swe}/PS1ΔE9* leads to age-dependent tau tangles, which do not occur with the tau fragment alone (Tong Li, unpublished). For the first time, our group has provided strong evidence that Aβ oligomers can indeed precipitate tangle formation in wild-type human tau, and that tangle formation accelerates neurodegeneration and cognitive deficits compared to AD-mutant mice alone. Importantly, in this novel model Aβ appears to drive the formation of tangles in wild-type human tau, which then induces the pathological conversion of endogenous mouse tau that can spread throughout the brain. Additionally, this is the first evidence that tangle formation of wild-type human tau can occur in the mouse brain, and can, therefore, be studied and manipulated in this system. However, further experiments are required to truly establish that Aβ oligomers drive pathology and neurodegeneration in these models, rather than another factor related to the AD-linked mutations. For example, administration of Aβ-targeting antibodies in *APP/PS1/tau4R* mice at an early age should prevent tau tangle formation, and would establish Aβ as the causative agent.

In summary, recently developed mouse models now recapitulate both Aβ oligomer and tau tangle pathologies and allow more detailed study of the amyloid cascade hypothesis. However, as discussed previously, there is now strong evidence that Aβ and tau may be among many factors that can drive AD pathogenesis, particularly in sporadic AD cases. Therefore, experimental models are required that allow further study

of putative non-canonical pathogenic factors and their contributions to neurodegeneration. Increasing evidence indicates that nuclear depletion of TDP-43 may also contribute to AD pathogenesis in a large population of AD cases, as described above. If so, we hypothesize that depletion of TDP-43 should lead to selective vulnerability in populations of neurons affected by AD, and should accelerate neurodegeneration in an AD-linked mammalian context. To investigate these questions, we employed the tamoxifen-inducible Cre^{ER} recombinase system to conditionally ablate *Tdp-43* in forebrain neurons of wild-type and $APP_{swe}/PS1dE9$ mice. In order to manage the complexity of the experimental model, we did not include tau as a facet in these initial studies. In addition, our interest in modeling the earliest stages of AD pathogenesis was most consistent with examining potential interactions between TDP-43 depletion and Aβ, rather than with tau which is thought to occur at a later stage of disease[8]. We focused our studies on the hippocampus and layer V of the cortex, two regions where degeneration correlates strongly with cognitive decline in early AD[100,101].

METHODS

Mouse model

All experiments were performed under an approved protocol and complied with regulations of the Animal Care and Use Committee at Johns Hopkins University School of Medicine. Forebrain depletion of TDP-43 in the adult mouse (*mus musculus*) was achieved by generating novel *CaMKIIα-Cre*^{ER};*Tdp-43*$^{F/F}$ (cT) mice with *loxP* sites flanking *Tdp-43* exon 3, allowing tamoxifen-induced recombination in excitatory forebrain neurons at maturity (Fig. 1a). Mature forebrain depletion of TDP-43 is consistent with the late onset of AD and regional specificity of neurodegeneration and TDP-43 proteinopathy in patients[40,102–105]. It is also necessary for these studies because constitutive knockout of TDP-43 is embryonically lethal, and heterozygous knockout does not reduce the levels of TDP-43 protein[60]. *CaMKIIα*-Cre^{ER};*Tdp-43*$^{F/F}$ (cT) mice were generated and bred with the *APP*$_{swe}$*/PS1dE9* (AP) line (purchased from Jackson Labs) to generate a cohort of *CaMKIIα*-Cre^{ER};*Tdp-43*$^{F/F}$;*APP*$_{swe}$*/PS1dE9 (*cTAP*)* mice on a C57BL/6J background, as well as littermate controls. Our breeding strategy is described in Fig. 1b. We utilized females exclusively because of sex differences in the AP mouse model[106,107]. Animals were genotyped at weaning, and animals of the genotype of interests were kept along with an equal number of littermate controls (4 mice/cage), and other pups in the litter were sacrificed. Oral tamoxifen was administered at an average 40mg/kg/day for a four week period beginning at p42-46, after mice reached developmental maturity[108]. This resulted in depletion of TDP-43 in the forebrains of mice carrying *CaMKIIα*-Cre^{ER};*Tdp-43*$^{F/F}$. No other tests, drug administration, or surgery were performed on these animals.

Studies were conducted in brain tissue from mice aged 3 to 14 months, collected from >30 litters over 15 months. At the appropriate age, mice were deeply anesthetized using 200μL/25g of 15% chloral hydrate, then perfused briefly with ice cold PBS. The brains were removed and one hemisphere was post-fixed in 4% paraformaldehyde for 24 hours. The other hemisphere was dissected into regions (cortex, hippocampus, cerebellum) and individually stored at -80°C. For electron microscopy, one animal of each genotype was perfused with 4% paraformaldehyde following the PBS perfusion. The brains were removed and placed in 4% paraformaldehyde + 2% glutaraldehyde for 18 hours. A <3mm^3 region containing the CA1 was then dissected out and processed for electron microscopy using standard procedures by the Johns Hopkins School of Medicine Microscope Facility Core.

Immunoblot and ELISA

Hippocampal tissue was homogenized in 10 volumes of ice cold RIPA buffer supplemented with 1x Protease inhibitor cocktail (Roche) and 1x phosphatase inhibitor (PhosSTOP), followed by centrifugation at 12,000xg for 20 min at 4°C. Alternately for ELISA, hippocampal tissue was homogenized in 8 volumes of 5M Guanidine HCl, then processed for ELISA using the Thermo Fisher human Aβ 42 kit (KHB3441) according to the manufacturer's instructions. Protein levels in the supernatant were determined using the BCA assay and 15μg of protein was loaded onto 4-12% or 10% Bis-Tris gels (Novex) along with 10uL SeeBlue Plus 2 pre-stained protein standard (Thermo Fisher), and transferred onto PVDF membrane. Membranes were probed with antibodies to synaptophysin (1:15,000, Abcam SY38/ab8049], PSD-95 (1:5000, NeuroMab K28/43), gephyrin (1:1000, BD Transduction Labs 610585), β-tubulinIII (1:30,000, Sigma T2200),

Cox1 (1:1000, Thermo Scientific PA5-26688), Tecpr1 (1:2000, Cell Signaling D6C10), Atg5-12 (1:1000, Cell Signaling D1G9), LC3B (1:1000, Sigma L7543), GSK3α[pY^{279}]/β[pY^{216}] (1:5000, Invitrogen 44604G), and Atg7 (1:2500, R&D Systems MAB6608). Band densitometry was quantified using ImageJ software on unaltered images, and normalized to total protein loaded using ponceau stain, unless otherwise noted. All samples were run at least twice to confirm consistency of the assay and validity of the observed effect; each data point represents the average of two independent blot results.

To assess the levels of pre-fibrillar and fibrillar oligomers we used the conformation specific antibodies A11 (Invitrogen AHB0052) and OC Millipore AB2286), respectively[109]. We homogenized cortex tissue in PBS + 1x Halt protease inhibitor (Thermo Fisher) at 4.5 months of age, when AP mice have visible plaque but cTAP mice do not. Homogenates were centrifuged at 100,000xg to isolate soluble oligomers[109], and supernatant was spotted onto membranes for standard dot blotting procedures.

Immunohistochemistry and Immunofluorescence

Brain hemispheres were post-fixed for 24hr in 4% paraformaldehyde, then removed to fresh PBS for 24hrs 2x. Hemispheres were sectioned in 10μm serial sections, then de-paraffinized and rehydrated. Antigen retrieval was performed in 10mM sodium citrate by boiling for 5 minutes, then endogenous peroxidases were inactivated with 0.3% sodium hydroxide for 30 minutes. Slides were blocked in 5% normal goat serum, or using the mouse on mouse staining kit (Vector Labs BMK-2202). Primary antibodies used were: 4G8 (1:1000, BioLegend 800702), TDP-43 N-terminal (1:500, Proteintech 10782-

2-AP) and SMI-31 (1:2000 IHC/ 1:1200 IF, Biolegend smi-31r). Secondary antibodies were either biotinylated for subsequent avidin binding and DAB reaction, or were conjugated to fluorescent epitopes (Alexa Fluor 488 and 564, 1:200).Hematoxylin or DAPI were used as nuclear counterstains.

Immunofluorescent images were taken on a Zeiss LSM 510 confocal microscope using a 63x oil objective in the Multiphoton Imaging Core of the Johns Hopkins School of Medicine, Department of Neuroscience. An Argon/2 laser was used for 488nm detection (transmission 24.8%, gain 541, amplifier offset, -0.017) and a DPSS laser was used for 561nm detection (transmission 37.8%, gain 621, amplifier offset -0.062).

Stereology

Brain volume, plaque burden and neuron counts were assessed using unbiased stereological methods with Stereo Investigator software. Brain region volumes were estimated using the Cavalieri probe (counting frame 150x150µm, grid spacing 200µm) in 3 sections/animal spaced 360µm apart. Plaque burden was estimated using the Area Fraction Fractionator probe (counting frame: cortex 300x350µm, cerebellum and hippocampus 200x250µm, grid spacing 15µm) in 3 sections/animal spaced 360µm apart. Neuron counts of hippocampal areas CA3/2, CA1 and DG were estimated by counting the number of neuron nuclei per region in 10 sections/animal spaced 150um apart. As all tissue was cut in 10µm thin sections, an optical disector method was not used, however, these hippocampal layers and neuronal nuclei sizes are highly uniform which minimizes the caveats of using a simple count.

RNA sequencing functional analysis

RNA sequencing data from *CaMKIIα-Cre*^{ER};*Tdp-43*$^{F/F}$ mice were obtained from Jeong *et al*. (unpublished). The following exclusion criteria were applied to generate a list of the most affected gene products: genes were excluded if the cryptic exon was not included in at least 50% of the total RNA generated, or if the RNA fold-change was greater than 1.5. These changes reduced the dataset to either heavily downregulated RNAs or those with an RNA population containing at least 50% of the cryptic exon; qualities that make them more likely to exert a functional effect on the cell. These exclusion criteria reduced the list from >100 transcripts to 30. The functional categories of the corresponding genes were determined by a manual literature search and are presented in Table 1. Three genes had unclear functions and were excluded from the final list.

Randomization and blinding

All animals received tamoxifen treatment. No randomization was used to assign animals to groups for data collection and processing. Rather, animals of each genotype were collected at the appropriate age in batches containing approximately equal representation of each genotype. Tissue from each age group was processed in a single batch when possible, or in multiple batches containing equal numbers of animals from each genotype. During data collection and analysis, the investigator was blinded to genotype by assigning an unrelated individual number to each animal at weaning.

Statistical analysis

Sample power calculations were performed using SPSS Sample Power 3.0. Between groups we were interested in measuring mean differences of at least 25%, and

estimated a standard deviation of 15%. Using these criteria, a per group sample size of 8 animals has an estimated 87% power. For larger mean differences of at least 40%, a per group sample size of 5 animals has an estimated 96% power. Therefore, for most statistical analyses the final sample size was $n>8$, and all were $n\geq5$. Specific sample sizes for each graph are reported in legends, and represent biological replicates (# mice/group). Data were organized and analyzed using SPSS Statistics 23.0. Data were analyzed with Univariate ANOVA by genotype within each age group. A *4(genotype) x 3(age)* design could not be used due to violations of heterogeneity of variances across age groups. Boxplots showed the median, interquartile range (box) 1.5 interquartile range (whiskers), outliers (○), and extreme cases (◊) of individual variables for each genotype. Normality was validated by ensuring that the $|skew/standard\ error\ skew|<2$ for each group, and Welch's test was used instead of ANOVA if normality was violated in one or more groups. When dependent variables were found significant across genotypes, we used Gabriel post-hoc tests (as groups had slightly unequal sample sizes), or Games-Howell when homogeneity of variances was violated. Post-hoc comparisons are paired with "wt", unless otherwise specified. Unpaired t-tests (two-tailed) are reported when only two groups are compared. For linear regression analysis, R^2 values and ANOVA significance values are reported. For western blots, occasional bands were not quantified *a priori* due to smearing or bubble artifacts that would disrupt the accuracy of quantification. For all studies, no data points were removed from analysis.

RESULTS

Large pyramidal neurons in the cerebral cortex and hippocampus are selectively vulnerable to depletion of TDP-43

It has long been recognized that certain large pyramidal neurons, including those of the hippocampal CA1 and frontal cortex layer V, are selectively vulnerable to neurodegeneration in AD[100,101]. To determine whether these neuronal populations are also more sensitive to depletion of TDP-43, we employed the tamoxifen-inducible *Cre*^{ER} recombinase system to conditionally ablate *Tdp-43* in forebrain neurons. Mice with floxed *Tdp-43* alleles[60] were crossed with the *CaMKIIα-Cre*^{ER} driver line to generate *CaMKIIα*-Cre^{ER};*Tdp-43*$^{F/F}$ (cT) mice (Fig. 1a). Administration of tamoxifen in adult cT mice led to depletion of TDP-43 in ~80% and ~30%, respectively, of hippocampal pyramidal and layer V frontal cortical neurons (Fig2. a-c).

Figure 1. Generation of mice with TDP-43 depletion and *APP$_{swe}$/PS1dE9* mutations**.** (**a**) Gene diagram of *CaMKIIα*-Cre^{ER} and *Tdp-43*$^{F/F}$ alleles. Administration of tamoxifen leads to cre-mediated excision of *Tdp-43*. (**b**) Breeding strategy for generating *CaMKIIα-Cre*^{ER};*Tdp-43*$^{F/F}$;*APP$_{swe}$/PS1dE9* mice and littermate controls. (#) indicates the Mendelian frequency of pups from each litter expected to carry the genotype of interest.

Figure 1.

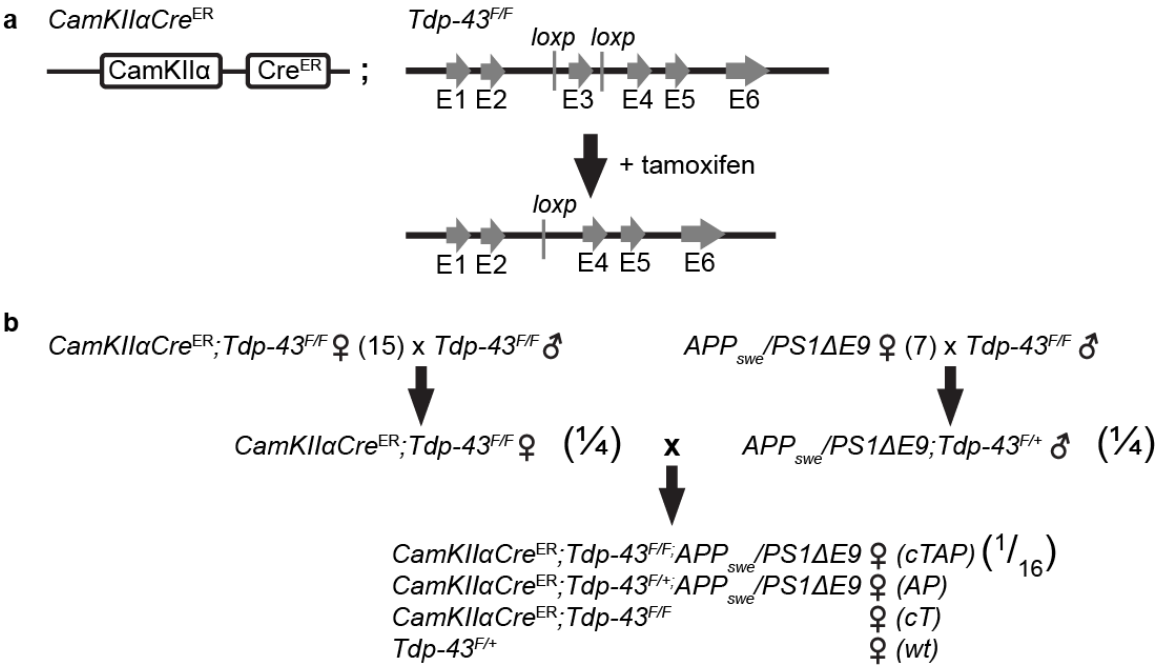

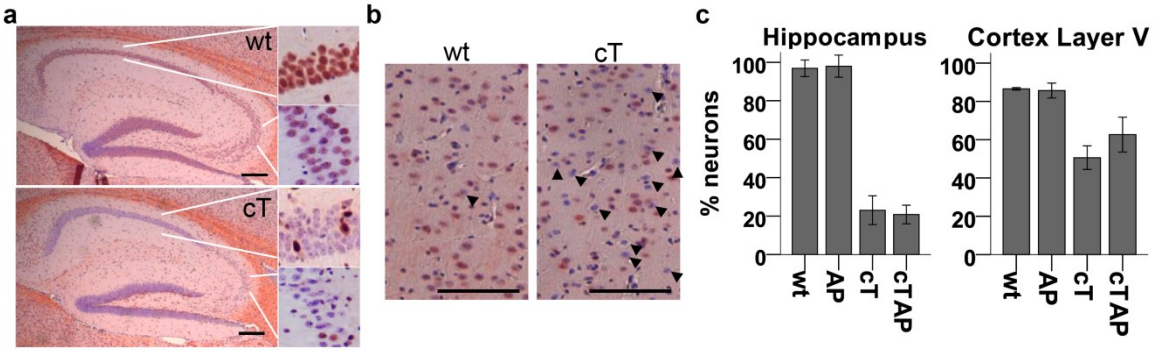

Figure 2. TDP-43 depletion in the cortex and hippocampus of cT mice. (**a,b**) TDP-43 (red) with hematoxylin counterstain (blue) for representative AP and cTAP sections in the (**a**) hippocampus and (**b**) cortex. (**c**) Quantifications of % neurons retaining TDP-43 staining for each genotype. Arrowheads indicate some neurons without visible TDP-43 staining. Scale bars (**a**)=200 μm (**b**)=100 μm.

Depletion of TDP-43 led to progressive age-dependent forebrain atrophy in the hippocampus, cortex, and corpus callosum (Fig. 3a,d). As expected, the volume of the cerebellum remained normal (Fig. 3d), since TDP-43 is not depleted in this region. Interestingly, we observed early selective vulnerability to depletion of TDP-43 in hippocampal CA3/2 (Fig. 3b,e) and cortical Layer V (Fig. 3c,f) neurons. Pathological accumulation of phosphorylated neurofilament[110] was evident in layer V neurons lacking TDP-43 as early as 3 months (Fig. 3f,g) and >50% of these neurons degenerated by 4 months of age (Fig. 3c, graph not shown) [t(10)=7.029, $p<0.001$, wt (*M=868, SD=78*), cT (*M=385, SD=137*), n: wt=5, ct=7]. In the hippocampus, 40% of CA3/2 neurons were lost by 6 months (Fig. 3e). One interpretation of these findings is that some regions vulnerable to depletion of TDP-43 are also vulnerable in human AD (i.e. frontal cortex layer V), while others may be distinct (i.e. hippocampus CA3/2 in mouse vs. CA1 in human). Another possibility is that the apparent difference in hippocampal selective vulnerability is actually due to differences in the distribution of neurons with TDP-43 nuclear depletion in human AD vs our cT mouse model. While cT mice have depletion of TDP-43 in >80% of all hippocampal neurons, human AD brains have depletion of TDP-43 only in a small subset of neurons, and current evidence suggest they are unevenly distributed in throughout the hippocampal layers[111,112]. Further studies are required to determine the frequency of TDP-43 depletion in each hippocampal region of AD cases, and whether selective vulnerability is indeed appreciable in any region.

Figure 3. TDP-43 LOF leads to progressive forebrain atrophy and selective vulnerability in hippocampal CA3/2 and cortical Layer V neurons. (**a-c**) Representative cresyl violet stained sections. (**a**) Progressive hippocampal and cortical atrophy in cT mice, with cortical thinning and severe CA3/2 cell loss (arrows). (**b**) Selective degeneration of CA3/2 neurons in cT mice (some indicated by arrows) at 4 months, while CA1 and DG are unaffected. (**c**) Numerous degenerating neurons in layer V (arrows) of cT mice at 4 months. (**d**) Regional volume in cT mice is reduced in hippocampus (Hp) [$F(1,11)=18.836$, ***$p=0.001$], cortex (Ctx) [$F(1,11)=46.435$, ***$p<0.001$], and corpus callosum (CC) [$Welch(1,5.505)=19.470$, **$p=0.001$], but not cerebellum (Cb) [$F(1,11)=0.066$, $p=0.803$], compared to wt (wt n=5, ct n=8). (**e**) CA3/2 neurons are selectively lost at 6 months [$t(10)=3.428$, **$p=0.002$; wt (M=182.42, SD=54.41), cT (M=104.62, SD=11.37)], followed by the dentate gyrus (DG) at 14 months ($t(14)=2.339$, *$p=0.035$) while CA1 neurons are unchanged [$t(14)=1.843$, $p=0.087$]. (3m and 6m n=6; 14m n=8). (**f**) Pathologic accumulation of phosphorylated neurofilament (SMI31, arrows) occurs in layer V neurons in cT mice at 3 months (arrows). (**g**) Co-staining of TDP-43 (yellow) and SMI31 (red) shows neurons with neurofilament pathology are depleted of TDP-43 (arrowheads). Scale bars (**a**)=200 μm (**c**)=100 μm (**b,f,g**)=50 μm.

Figure 3.

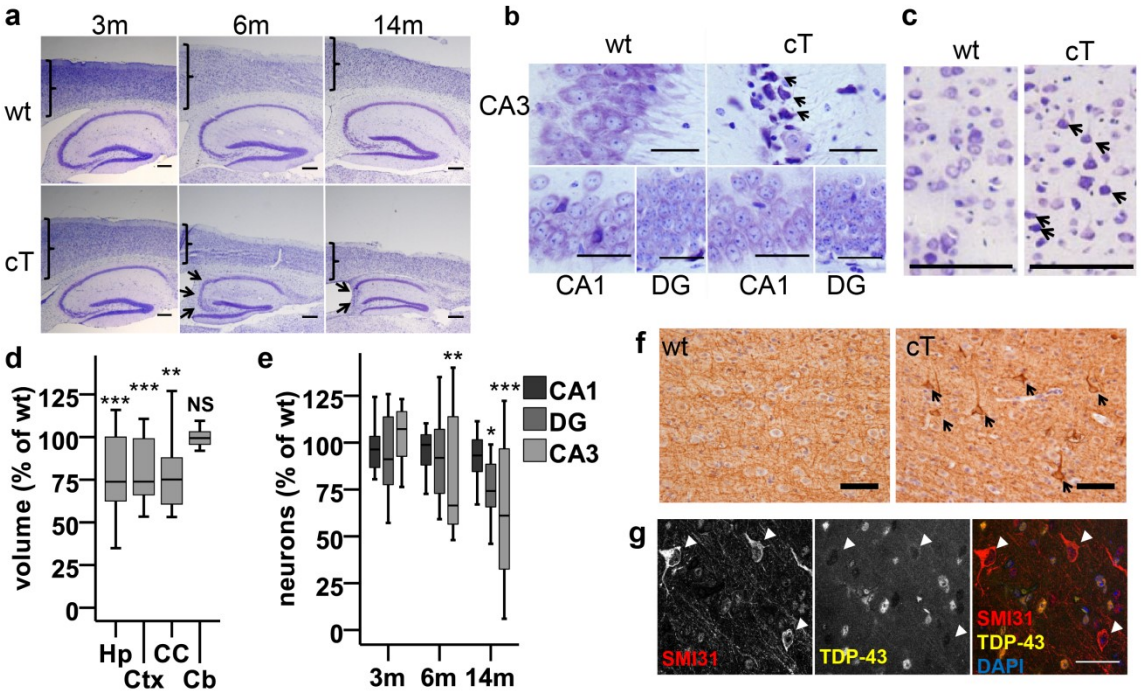

Depletion of TDP-43 in forebrain neurons accelerates neurodegeneration in *APP$_{swe}$/PS1ΔE9* mice

Previous work has shown that TDP-43 proteinopathy in AD cases correlates strongly with worsened cognition compared to AD cases without this pathology[52]. However, it remains unclear whether nuclear depletion of TDP-43 accelerates neurodegeneration and cognitive decline, or whether it merely occurs alongside these deficits. To assess whether nuclear depletion of TDP-43 might accelerate neurodegeneration in AD, we crossed *CaMKIIα-Cre^{ER};Tdp-43$^{F/F}$* (cT) mice with AD-linked *APP$_{swe}$/PS1ΔE9* (AP) mice to generate *APP$_{swe}$/PS1ΔE9* mice lacking Tdp-43 in forebrain neurons (cTAP) (Fig. 1b). Though *APP$_{swe}$/PS1ΔE9* mice lack frank neuron loss, they exhibit significant synaptic and mitochondrial degeneration[87,113], pathological features that are well-suited to assess accelerated neurodegeneration in an AD-related

context. As expected, the expression of *APP_{swe}/PS1ΔE9* had no additional effect on the rate of *Tdp-43* excision (Fig. 2c).

Histological and electron microscopical analysis revealed numerous CA1 pyramidal neurons with markedly swollen, empty cytoplasm in cTAP mice compared to control littermates, suggesting degenerating neurons (Fig. 4; Fig. 5a-c). In addition, some cTAP animals also showed occasional darkly stained pyknotic cells within the CA1 layer and severe vacuolation of the stratum radiatum (Fig. 4), while these abnormalities were absent from cT and AP mice. Accelerated neurodegeneration in cTAP mice was further confirmed by morphological analysis, judged by severe swelling and dystrophy in mitochondria and Golgi/ER, and cytoplasmic discontinuity with loss of ribosomes (Fig. 5b,c).

Figure 4. Severe degenerative phenotypes are visible in cTAP mice compared to littermate controls. Representative series of H+E stained sections from 5 mice/genotype. Degenerating neurons with pale staining cytoplasm (some indicated by arrows) are especially numerous in cTAP mice compared to littermate controls at 8 months. In addition, a subset of cTAP mice (#2, 4+5) display severe vacuolation (*) of the CA1 stratum radiatum (sr) and stratum oriens (so) while littermate controls have only occasional vacuoles. Scale bars=100 μm.

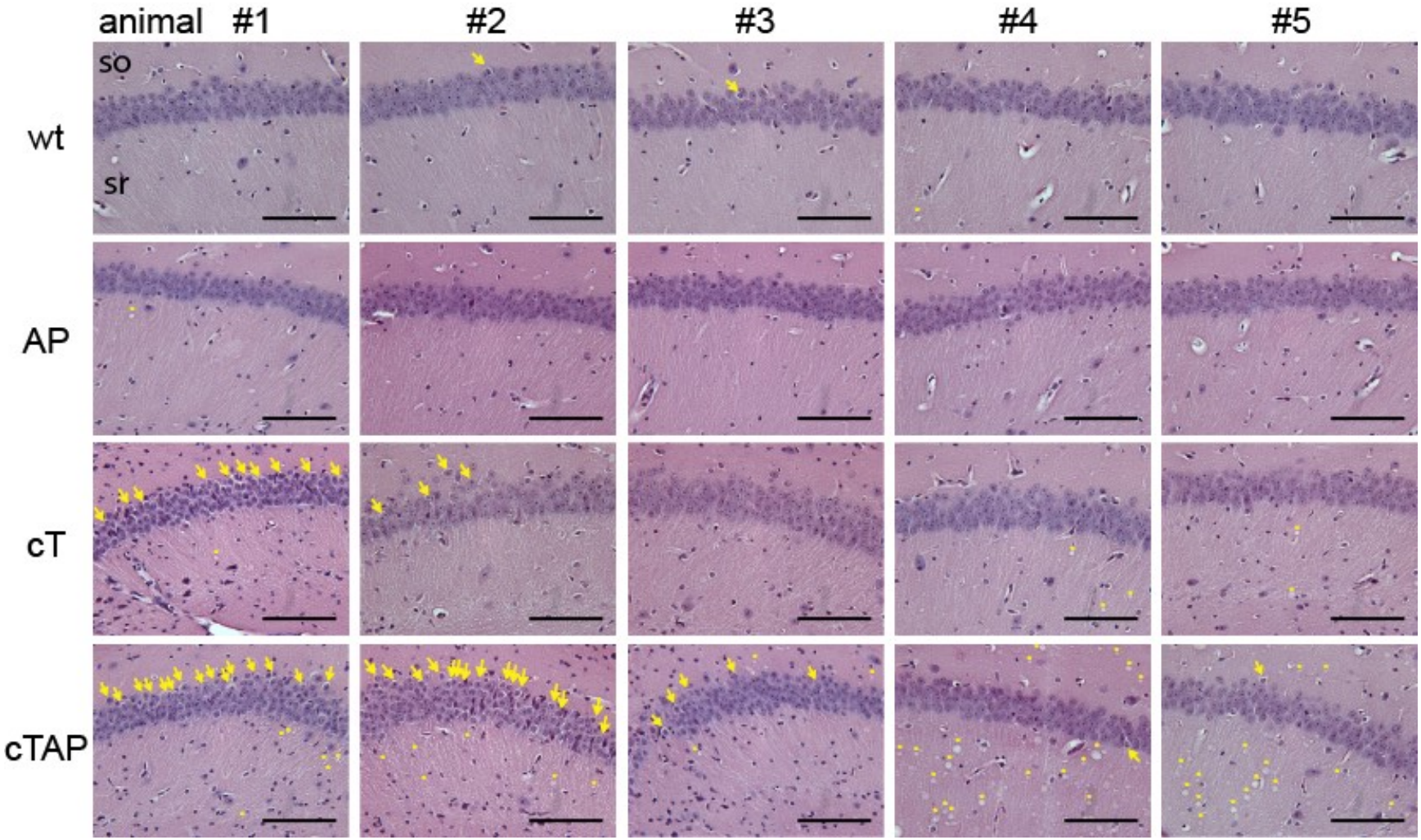
animal #1
#2
#3
#4
#5
so
sr
wt
AP
cT
cTAP

Figure 5. Depletion of TDP-43 accelerates neurodegeneration in *APP/PS1* mice. (**a**) H+E staining: numerous CA1 pyramidal neurons show pale staining cytoplasm in 8 month cTAP mice (bottom), in contrast to normal cytoplasm of AP (top) and most cT (middle) neurons. Occasional darkly stained pyknotic cells are also visible in cTAP mice. Scale bars=100 μm. (**b**) Electron micrographs from CA1 pyramidal neurons at 6 months show sparsely populated and discontinuous cytoplasm (yellow) with loss of ribosomes (**c**, boxed) in cTAP mice, compared to cT and AP littermates (n=1 animal/group). Dystrophic organelles, including mitochondria (**b**, red; **c**, arrows), and Golgi/smooth ER (**b**, green) are most severe in cTAP mice. Dystrophic neurites (pink) only occasionally contain lysosomes (black). Scale bars=2 μm. (**d**) Mitochondrial Cox1 is reduced in cTAP [$F(3,26)=3.044$, $p=0.047$, Gabriel $^{*}p=0.033$], but not AP (Gabriel $p=0.462$) or cT mice (Gabriel $p=0.397$), compared to wt littermates at 4 months. (wt=9, AP=11, cT/cTAP=10). (**e)** Lysosomal Tecpr1 is reduced in TDP-43 depleted mice compared to AP at 4 months [$F(3,31)=14.322$, $p<0.001$; Games-Howell cT $^{***}p<0.001$, cTAP $^{*}p=0.017$] (wt n=8; AP, cT, cTAP n=9). Its autophagosomal binding partner Atg5-12 is also reduced in 8 month cTAP mice compared to AP [$F(3,20)=11.902$, $p<0.001$; Gabriel $^{***}p<0.001$] and cT (Gabriel $^{*}p=0.016$), while another autophagosome protein Atg7 is not [$Welch(3,9.619)=1.680$, $p=0.236$]. GSK3 is significantly increased in 8 month cTAP [$F(3,20)=7.012$, $p=0.002$; Gabriel $p=0.006$] but not AP ($p=1.000$) or cT ($p=0.242$) mice compared to wt littermates. (4m: wt n=6, AP n=7, cT n=11, cTAP n=10; 8m: wt n=5, AP n=6, cT n=7, cTAP n=6). (**f**) Synaptophysin (Syp) is reduced in 8 month cTAP mice compared to AP [$F(3,20)=8.860$, $p=0.001$; Gabriel $^{**}p=0.003$) and cT (Gabriel $^{*}p=0.048$). PSD95 and Gphn do not show accelerated changes, though PSD increased in all transgenic genotypes [$Welch(3,9.648)=40.973$, $p<0.001$; Games-Howell AP $^{***}p<0.001$, cT $^{**}p=0.002$, and cTAP $^{**}p=0.007$] compared to wt at 8 months. β-tubulin-III is reduced in 8 month cTAP [$F(3,20)=5.640$, $p=0.006$; Gabriel $^{**}p=0.007$], but not AP (Gabriel $p=0.290$) or cT (Gabriel $p=0.952$) mice compared to wt. (4m: wt=9, AP=11, cT/cTAP=10; 8m: wt=5; AP=6; cT=7, cTAP=6) Outliers (○), and extreme cases (◊).

Figure 5.

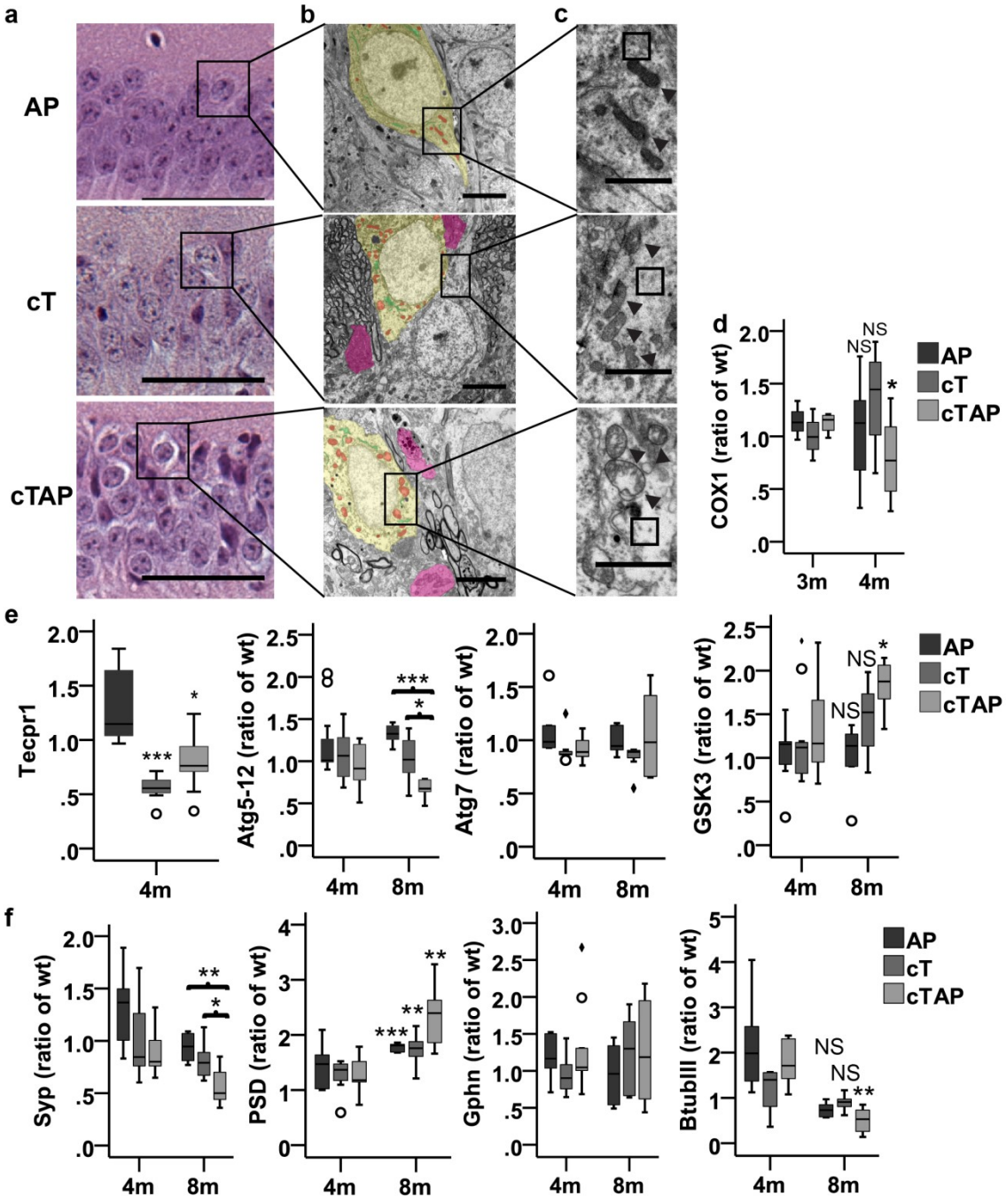
a
b
c
AP
cT
cTAP
d
COX1 (ratio of wt)
NS
NS
*
AP
cT
cTAP
3m
4m
e
Tecpr1
***
*
Atg5-12 (ratio of wt)
***
*
Atg7 (ratio of wt)
GSK3 (ratio of wt)
NS
NS
*
4m
8m
f
Syp (ratio of wt)
**
*
PSD (ratio of wt)
***
**
**
Gphn (ratio of wt)
BtubIII (ratio of wt)
NS
NS
**

We showed previously that depletion of TDP-43 leads to the incorporation of aberrant cryptic exons, and usually subsequent degradation of the associated mRNAs[68]. To assess the possible contribution of these cryptic exons to accelerated neurodegeneration in cTAP mice, we performed functional pathway analysis on the RNAs most likely to be strongly affected by TDP-43 depletion. RNA sequencing data was generated from *CaMKIIα-Cre*^{ER};*Tdp-43*$^{F/F}$ mouse brains and non-transgenic littermates (Jeong et al., in review). Genes were selected for functional analysis if the cryptic exon was included in at least 50% of the total RNA generated, or if the RNA fold-change was greater than 1.5.; qualities that make them more likely to exert a meaningful effect on neuronal function. The functional categories of these genes were determined by a manual literature search (Table 1). Six genes had predominantly developmental functions, and three genes had unclear functions and were excluded from the final table. These exclusion criteria reduced the list from >100 transcripts to 20. Importantly, we identified three pathways strongly implicated in the pathogenesis of AD that are also affected by cryptic exon incorporation: synaptic signaling[8,114], mitochondrial function[113,115], and autophagy[116] (Table 1). We examined essential components of these three pathways to further confirm accelerated neurodegeneration in the hippocampus of *CaMKIIα-Cre*^{ER};*Tdp-43*$^{F/F}$;*APP*$_{swe}$*/PS1ΔE9* mice.

Table 1. Functional pathways of selected transcripts containing TDP-43-associated cryptic exons that are most likely to exert a functional effect on neurons. The selection procedure is described fully in the Methods. Genes are color coded by strength of downregulation (blue) or upregulation (red) of their RNA products. Increasing intensity of color indicates a stronger effect. Pathways in bold have been strongly implicated in the pathogenesis of AD.

Synaptic/ secretory	**Mitochondrial**	**Autophagy**	General signaling (TGFβ, NFκB, calcium)	Immune response	Transcription/ translation
Cacna1b	Mrps6	Tecpr1	Usp15	Crlf1	Brms1l
Cdh22	Synj2bp		Camk1g		Celf5
Dlg3			Crem		
Fxyd2					
Kcnmb4					
Pitpnm3					
Ralgps2					
Src					
Rgs17					
Unc13a					
Vps13d					

In mitochondria, we observed a significant loss of Cox1, an essential component of the electron transport chain, in cTAP mice compared to littermate controls (Fig. 5d). In the autophagy pathway, we previously reported that *Tecpr1*, critical for fusion of autophagosomes to lysosomes[117], is a major target of TDP-43 in the brain (Jeong et al. in review). Further, protein levels of Tecpr1 were indeed reduced in mice lacking TDP-43 (Fig. 5e). Tecpr1 binds the Atg5-12 complex[117,118], and depletion of Atg5 has been shown to cause neurodegeneration *in vivo*[119]. Notably, Atg5-12 was also reduced in cTAP mice compared to littermate controls by 8 months, while another essential autophagosome formation factor, Atg7, remained unchanged (Fig. 5e). The apparent specificity of this

downregulation suggests that incorporation of some TDP-43-associated cryptic exons may impair neuronal function directly. Finally, the pre-synaptic vesicle protein synaptophysin was reduced in cTAP mice at 8 months compared to littermate controls (Fig. 5f), as was the axonal structural marker β-tubulin-III (Fig. 5f). Post-synaptically, no significant differences were found in excitatory (PSD-95) or inhibitory (gephyrin) post-synaptic scaffolds (Fig. 5f), consistent with observations that presynaptic terminals are initially affected in cases of AD[120]. Together, our data suggest that pathways impacted by cryptic exon incorporation due to nuclear depletion of TDP-43 contribute to neurodegeneration in cases of AD with TDP-43 pathology, and may open the door to new therapeutic opportunities.

Interestingly, active GSK3, a kinase that promotes autophagosome formation[121], was increased in cTAP mice compared to littermate controls (Fig. 5e), though autophagosome formation factors themselves were either decreased (Atg5-12) or unchanged (Atg7) and no autophagosomal pathology was seen by EM. This apparent contradiction may reflect an attempt by TDP-43 depleted neurons to compensate for a deficit in autophagy by increasing signaling that promotes this pathway. Notably, increased GSK3 activation is well-documented in AD cases[122], suggesting that this finding in cTAP mice warrants further study. Further experimental manipulation of the autophagy pathway in neurons with nuclear depletion of TDP-43 will help unravel its consequences on autophagy and may shed light on important mechanisms of AD pathogenesis.

Though our data would seem to suggest that mitochondrial degeneration occurs first in cTAP mice at 4 months, followed by defects in autophagy and synaptic signaling

by 8 months, the complexities of the latter pathways do not allow us to make strong conclusions about the timeline of degenerative processes. For example, compensatory axon sprouting has been shown in mice carrying AD-linked mutations[123,124] that could mask degeneration of synaptic terminals. Therefore, future detailed studies would be of interest to establish the order, or simultaneous onset, of degenerative mechanisms due to TDP-43 depletion in AD, and may provide useful information for the development of therapeutics and our understanding of AD pathogenesis.

Accelerated neurodegeneration in *APP_{swe}/PS1ΔE9* mice with depletion of TDP-43 is independent of the Aβ plaque burden

Unexpectedly, while depletion of TDP-43 in *APP_{swe}/PS1ΔE9* mice accelerated neurodegeneration, it also significantly reduced Aβ plaque burden (Fig. 6a,b). In addition, the relative level of fibril vs. pre-fibril oligomers was also significantly reduced in forebrain homogenates of cTAP compared to AP mice (Fig. 6c,d). These data indicate that the accelerated neurodegeneration occurring in cTAP mice is independent of the Aβ plaque burden or fibrillar Aβ oligomers. Importantly, the total levels of Aβ42 were unchanged in the forebrains of cTAP mice compared to littermate controls (Fig. 7a). Simple linear regression for dependence modeling of a variable demonstrated that the reduced plaque density was also not significantly explained by volume loss (Fig. 7b). Finally, the levels of the Aβ precursor protein (APP) and the proteases that cleave it, PS1 and BACE1, were all unchanged in cTAP mice compared to AP littermates. These findings indicate that the reduced burden of fibrillar and plaque Aβ is not due to simple changes in Aβ production, and may reflect an important mechanistic effect of TDP-43

depletion on Aβ dynamics and other neuronal functions. Future experiments would be of great interest to uncover whether depletion of TDP-43 might alter processes like Aβ fibrilization, secretion, or degradation. In addition, experimentally depleting TDP-43 in the brain after Aβ plaque deposition has already begun would provide further information on the processes underlying Aβ plaque reduction in the current cTAP mouse model.

Figure 6. Accelerated neurodegeneration in cTAP mice is independent of Aβ plaques and fibrillar oligomers. (**a**) Representative series of 4G8 stained plaques (arrow, example) in 5 different animals/genotype at 8 months. The reduction in plaque burden in cTAP (bottom) compared to AP (top) mice is obvious by visual inspection. Scale bars=200 μm. (**b**) Plaque burden is significantly reduced in the forebrains of cTAP mice compared to AP littermates at 4 months [$F(1,16)=10.756$, $^{**}p=0.005$] and 8 months [$F(1,18)=30.329$, $^{***}p<0.001$]. (3m,4m n=9/group; 8m AP=9, cTAP=11). Outlier (○). (**c**) Representative dot blots of pre-fibril (A11) and fibril (OC) oligomers soluble in PBS after centrifuging at 100,00xg. (**d**) Relative levels of fibrillar oligomers (OC:A11) were significantly decreased in cTAP mice at 4 months [$F(1,10)=6.626$, $^{*}p=0.028$] (n=6). Outliers (○), and extreme cases (◊).

Figure 6.

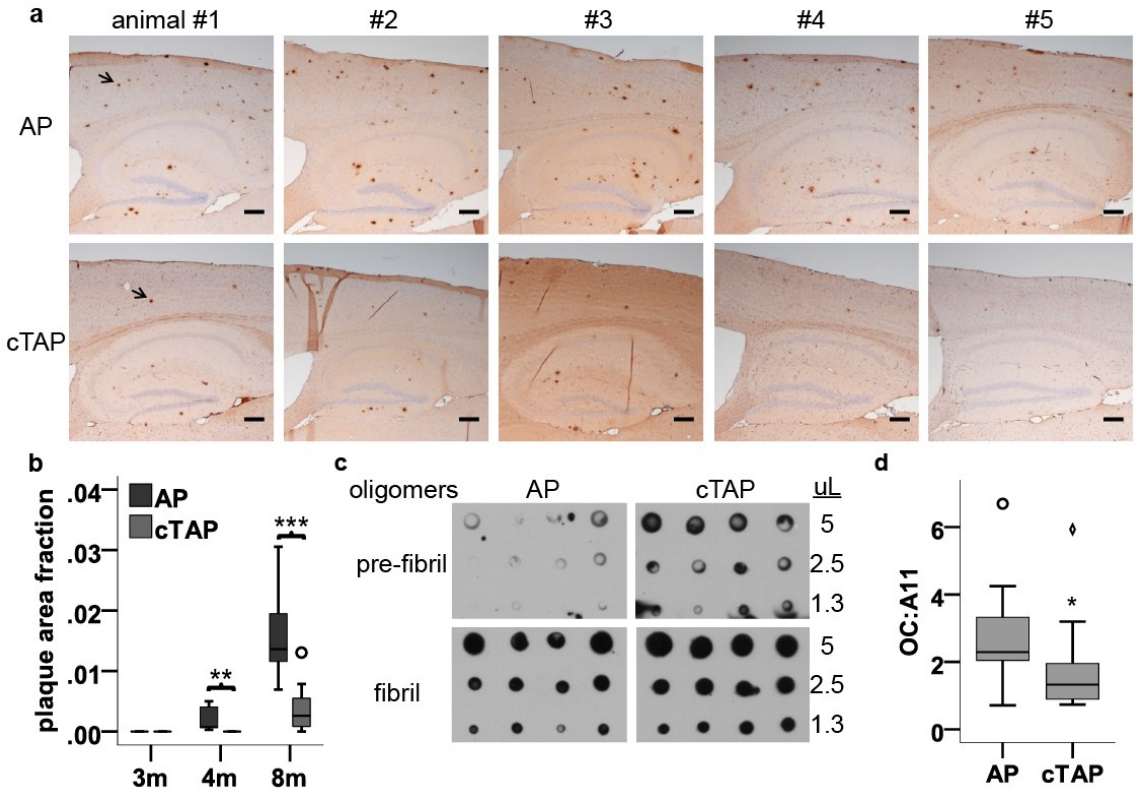

Together, our findings support a model whereby nuclear depletion of TDP-43 contributes to the pathogenesis of AD. This provides strong rationale to develop novel therapeutics to alleviate the depletion of nuclear TDP-43 and to create functional ante-mortem biomarkers for early detection. Additionally, our data are consistent with the view that non-fibrillar soluble forms of Aβ, rather than fibrils and plaques, facilitate neurodegeneration in AD[9,88]. Given the apparent importance of the conformational state of Aβ, the equilibrium relationship between different conformational states underscores a great challenge of designing effective of Aβ-directed therapeutics[125]. However, interim data from recent clinical trials showing that Aβ-directed antibodies derived from aged cognitively normal humans, such as Aducanumab (BIIB037, clinialtrials.gov), reduce

brain Aβ and halt cognitive decline indicate that harnessing the immune system may allow clinicians to safely lower multiple forms of Aβ simultaneously (presented at the 12th International AD/PD Conference, Nice, France, March 2015). Since nuclear depletion of TDP-43 may occur in a majority of AD cases[52], our findings suggest that stratifying AD subjects with TDP-43 pathology may greatly empower trials of promising Aβ-directed therapeutics.

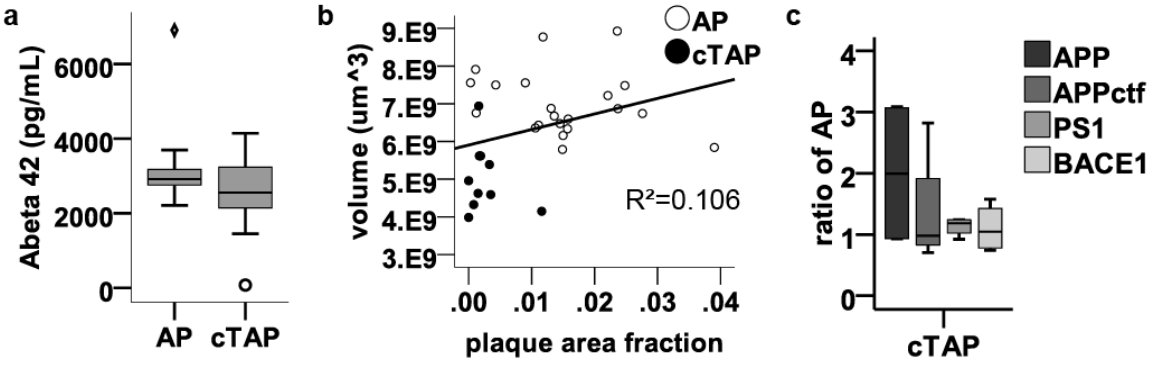

Figure 7. Reduced plaque burden is not explained by volume loss or lack of Aβ production. (**a**) Levels of Aβ42 were not changed in the forebrain of cTAP mice at 4 months [Welch(1,18.987)=2.584, *p=0.124*] (AP=11, cTAP=10). (**b**) Scatter plot of plaque area fraction vs. volume in the forebrain. Linear regression analysis revealed that volume loss does not contribute significantly to plaque area fraction (R^2=0.106; ANOVA F(1,29)=3.425, *p=0.074;* n=31). (**c**) Levels of the Aβ precursor protein (APP) and the proteases that cleave it, PS1 and BACE1, are all unchanged in cTAP compared to AP littermates. APP [F(1,11)=0.164, *p=0.694*] (AP=7, cTAP=6), PS1 [F(1,6)=1.540, *p=0.261*], BACE1 [F(1,6)=0.004, *p=0.950*] (AP=3, cTAP=5).

DISCUSSION

Together, our data support the hypothesis that depletion of TDP-43 contributes to the pathogenesis of AD in cases with TDP-43 proteinopathy. Previous work has established an essential role for TDP-43 in mammalian embryogenesis (Kraemer et al., 2010; Sephton et al., 2010) and vertebrate development (Schmid et al., 2013), as well as diverse roles during adulthood (Chiang et al., 2010) including neuron survival in the spinal cord (Wu et al., 2012; Iguchi et al., 2013; Yang et al., 2014). Importantly, we now show that in adult mice, depletion of TDP-43 is not equally toxic to all populations of neurons, as the frontal cortex layer V and hippocampal CA3/2 pyramidal neurons are selectively vulnerable to TDP-43 depletion in the forebrain, even compared to other large pyramidal neurons like those of the CA1. As we noted previously, further studies are required to determine whether the same pattern of selective vulnerability occurs in AD patients with TDP-43 proteinopathy. However, data from AD patients in general has shown that frontal cortex layer V neurons are indeed selectively vulnerable in the disease generally[100,101]. In the hippocampus, most data from AD cases (not stratified by TDP-43 proteinopathy) indicate that the CA1 is most vulnerable[126]. Re-examination of these datasets with stratification for TDP-43 proteinopathy would be of great interest, particularly datasets using histology with unbiased stereology that provide greater sensitivity than volumetric studies. However, the design and interpretation of these studies may be complicated by the fact that TDP-43 proteinopathy occurs only in a small subset of neurons that appear unequally distributed throughout hippocampal sub-regions (Uryu et al., 2008; Kadokura et al., 2009). Nevertheless, if depletion of TDP-43 does cause selective vulnerability in the CA3/2 in humans, AD cases with TDP-43

proteinopathy would have two populations of severely dysfunctional hippocampal neurons, which may contribute to the worsened cognition observed in these patients[52].

Second, we show that depletion of TDP-43 accelerates hippocampal neurodegeneration, while reducing Aβ fibrils and plaques in *APP_{swe}/PS1dE9* mice. Our data suggest that TDP-43 may accelerate neurodegeneration both directly, through incorporation of cryptic exons, and indirectly, by increasing non-fibril Aβ oligomers. Specifically, in the autophagy pathway we show that an autophagosome formation factor (Atg5-12) that is a binding partner of a downregulated TDP-43-associated cryptic exon target (Tecpr1) is also downregulated, while an unrelated autophagosome formation factor (Atg7) is not. However, further studies are required to rigorously evaluate the mechanisms by which depletion of TDP-43 contributes to AD. For instance, rescuing suppression of TDP-43 associated cryptic exons in cTAP mice and examining the degenerative phenotypes that can be prevented or rescued would test the hypothesis that failure to repress cryptic exons directly contributes to neurodegeneration. To that end, our group has developed a fusion protein coupling the RNA-binding domains of TDP-43 with the splicing repressor region of the RAVER1 protein, and have shown that it can suppress TDP-43-associated cryptic exons[68]. We can, therefore, use this construct to evaluate the contribution of cryptic exon suppression to the deficits observed with depletion of TDP-43.

Another important factor to consider in studying TDP-43-associated cryptic exons is that they are nonconserved, meaning that the genes containing cryptic exons vary between species[68]. Therefore, the genes affected by depletion of TDP-43 in our mouse model will have little to no overlap with those affected in human AD. Currently, our

group is working to uncover the cryptic exon targets of TDP-43 depletion in human neurons, which will allow a direct comparison of both the target genes and the pathways to which they belong. Therefore, although the specific genes will likely differ between mouse and human, the pathways they disrupt may overlap. Indeed, the original studies of the role of TDP-43 in splicing found that the incidence UG dinucleotide repeats to which TDP-43 binds increased with the length of introns[61], suggesting that UG repeats occur in a random manner throughout the genome. Therefore, pathways which are most crucial to neurons, and have the most genes associated with them, are also most likely to have an abundance of cryptic exons in any species. In this manner, the general mechanism by which depletion of TDP-43 contributes to AD may be conserved in mouse, although the particular gene targets are not conserved.

Whether the contributions of Aβ and depletion of TDP-43 are independent (acting on different pathways), synergistic (acting on the same pathways), or epistatic (one leads to the other) is highly relevant for development of therapeutic strategies. If the two contribute to neurodegeneration through a common mechanism, one therapeutic agent may be sufficient to halt or slow neurodegeneration in AD patients with multiple pathologies. However, our data suggest that TDP-43 may accelerate neurodegeneration through mechanisms that are at least partially independent of Aβ (though further studies are required to firmly establish this hypothesis). In addition, a recent clinico-pathologic study of aged individuals with and without dementia showed that the presence of one pathology (TDP-43 proteinopathy or Aβ plaques) did not make the other more likely to occur[47]. This suggests that Aβ- and TDP-43 dysfunction are likely not epistatic of each other. Importantly, if these dysfunctions represent separate mechanistic pathways, the

administration of therapies directed to either alone would be expected to produce minimal benefits in AD patients with TDP-43 proteinopathy. Given that up to 60% of AD cases have TDP-43 proteinopathy, we hypothesize that this situation may confound the evaluation of current Aβ-directed therapeutics, and that stratifying subjects with TDP-43 pathology could empower AD clinical trials.

As discussed previously, our data in cTAP mice suggest that Aβ and depletion of TDP-43 synergistically contribute to neurodegeneration in AD. However, we cannot rule out the possibility that another factor related to the AD-linked mutations, such as altered PSEN1 function, may be contributing to accelerated neurodegeneration in cTAP mice. To rigorously demonstrate that Aβ is indeed the key interactor, experiments are required to remove the Aβ from mice with familial AD mutations, for instance using anti-Aβ antibodies. If Aβ is the true catalytic factor then the degenerative differences demonstrated here between cT and cTAP mice should not be present in cTAP mice treated with Aβ antibodies from an early age. Currently available human-derived Aβ antibodies, such as Aducanumab[127], which are currently in clinical trials, provide a therapeutically relevant choice for these experiments.

Our study is an important step in investigating the multiple mechanisms that may contribute to sporadic AD, which will aid the development of effective therapeutics. However, therapeutic success will depend heavily on our understanding of disease mechanisms and on the rigor of pre-clinical investigations. The recent failures of the γ-secretase inhibitor semagacestat were a strong reminder of the dangers of rushing to clinical trial, as the drug worsened cognition in AD patients instead of improving it, and strongly increased the risk of other adverse health outcomes including skin cancer[128].

Since Notch-related adverse events also occur in mice with inactivation of γ-secretase[129–131], and subsequent evidence has shown that semagacestat preferentially inactivates Notch over APP[132], more careful preclinical evaluation should have prevented this unfortunate failure. However, despite this recent reminder, another drug, bexarotene, is now in clinical trials despite the inability of several independent groups[133–136], including ourselves ([107], Appendix A), to consistently replicate the benefits reported in the initial study[137]. In addition to the potential damage to patients, clinical trials are expensive and time-consuming, and testing a drug that preclinical data indicates is likely to fail wastes limited resources. Additionally, failure of an ill-chosen drug makes it more difficult for other, potentially effective drugs of the same class to gain approval, as is now the case with γ-secretase inhibitors in general due to the failure of semagacestat in particular[138].

Our work provides strong rationale to develop novel therapeutics to alleviate the depletion of TDP-43 and to create functional ante-mortem biomarkers for early detection. Rescue of TDP-43-associated cryptic exon suppression may represent a viable therapeutic option for AD and other neurodegenerative diseases with TDP-43 proteinopathy, and we have begun preclinical evaluation of this hypothesis. As we discuss above, one important step in this evaluation includes experiments that establish the contribution of cryptic exon suppression to TDP-43 depletion-related neurodegeneration. The effects of cytoplasmic TDP-43 aggregation may also be relevant to disease and should be investigated. Finally, the mechanisms by which TDP-43 and Aβ may interact to cause neurodegeneration will be highly relevant, and will require carefully designed studies, as discussed previously. Together, these and other approaches

will increase our knowledge of AD pathogenic mechanisms, and aid the rational development of effective therapeutic strategies.

REFERENCES

Appendix A

Treatment with bexarotene, a compound that increases apolipoprotein-E, provides no cognitive benefit in mutant *APP/PS1* mice.

Katherine D. LaClair [†1, 4], Kebreten F. Manaye [†5, 6], Dexter L. Lee[5, 6], Joanne S. Allard[5, 6], Alena V. Savonenko[1, 3], Juan C. Troncoso[1, 3*], Philip C. Wong[1, 2, 4*]

Depts. of [1]Pathology, [2]Neuroscience and [3]Neurology, and [4]Program in Cellular and Molecular Medicine, The Johns Hopkins University School of Medicine. Depts. of [5]Physiology and [6]Biophysics, Howard University College of Medicine. Baltimore, MD 21205.

[†] These authors contributed equally to this work.

Background: Though the precise cause(s) of Alzheimer's disease (AD) remain unknown, there is strong evidence that decreased clearance of β-amyloid (Aβ) from the brain can contribute to the disease. Therapeutic strategies to promote natural Aβ clearance mechanisms, such as the protein apolipoprotein-E (APOE), hold promise for the treatment of AD. The amount of APOE in the brain is regulated by nuclear receptors including retinoid X receptors (RXRs). Drugs that activate RXRs, including bexarotene, can increase APOE and ABCA1 production, and have been shown to decrease the Aβ burden and improve cognition in mouse models of Aβ amyloidosis. Although recent bexarotene studies failed to replicate the rapid clearance of Aβ from brains, behavioral and cognitive effects of this compound remain controversial.

Findings: In efforts to clarify these behavioral findings, mutant *APP/PS1* mice were acutely dosed with bexarotene. While ABCA1 was upregulated in mutant *APP/PS1* mice treated with bexarotene, this drug failed to attenuate Aβ plaques or cognitive deficits in these mice.

Conclusions: We recommend rigorous preclinical study to evaluate the mechanism and utility of such a compound for AD therapy.

Keywords: Bexarotene, Alzheimer's disease, mouse model, RXR agonist, APOE, cognition

Introduction

The principle pathological characteristics of Alzheimer's disease (AD) include the extracellular deposition of β-amyloid (Aβ) plaques and intracellular aggregation of tau in the brain, abnormal synaptic function, and chronic inflammatory responses in neural tissue. A well-studied mouse model of Aβ amyloidosis is the double transgenic $APP_{swe}/PS1_{\Delta E9}$ mouse that exhibits Aβ plaques in the hippocampus and cortex beginning at 6 months of age (*1).* The progression of Aβ deposition occurs more rapidly in these transgenic females than in males (*2*). While Aβ has a clear link to AD – either directly or through the processing mechanisms of its precursor protein APP – Aβ is also present in healthy individuals in the form of low molecular weight soluble Aβ peptides that likely serve physiological roles (*3*). Levels of Aβ peptides are managed by clearance mechanisms in the brain that activate microglia to facilitate the removal of Aβ from the extracellular space (*4*). The most prominent of these clearance components is the

cholesterol transporter apolipoprotein-E (ApoE) because the *E4* allele as compared to that of *E2* or *E3* is the most significant risk factor for the development of non-familial (sporadic) AD. Individuals with *APOE4* have a pronounced increase in Aβ oligomerization (*5*) and AD incidence (*6,7*) relative to carriers of the other APOE alleles. *APOE4* has also been found to have decreased affinity for Aβ compared to *APOE3* or *APOE2*, but only when activated by lipidation (*8*), which implies that dysfunction in the regulation and action of APOE isoforms can play contributing roles in the pathogenesis of AD. The convergence of this data indicates that promoting APOE may be a productive therapeutic strategy in AD.

The transcription of *APOE* is facilitated by activation and heterodimerization of the nuclear receptor retinoid X receptor (RXR) with its partner receptors peroxisome activated receptors (PPARγ) or liver X receptors (LXR). These nuclear receptors also activate lipidators such as ABCA1 (*9, 10*), which appear necessary for the Aβ clearing abilities of ApoE (*8, 11, 12*). Therefore, a number of RXR agonists have been tested as a potential therapeutic mechanism of increasing Aβ clearance through ApoE. Bexarotene is one such agonist, which is selective for RXR and is FDA-approved for the treatment of cutaneous T-cell lymphoma. Cramer *et al*. (*13*) conducted studies with bexarotene in transgenic mouse models of Aβ amyloidosis. They reported that acute treatment with bexarotene upregulated ABCA1 and ApoE, rapidly reduced the Aβ plaque burden in the brain, and ameliorated cognitive deficits in these models. However, several groups have failed to replicate the effect of bexarotene on Aβ plaque burden in these and other related mouse models, despite achieving upregulation of the proposed targets ApoE and ABCA1 (*14,15,16,17*). While the original experiments were conducted on mouse models (*Tg2576*

and $APP_{swe}/PS1_{\Delta E9}$) that exhibit significant gender-related pathological differences (*18 and 2, respectively*), no distinction of gender was made in their analysis (*13*). In using a small cohort of mice in the studies, these gender differences could skew treatment groups leading to a false positive treatment effect. Moreover, gender-related differences are important in the evaluation of any RXR agonist or other compounds influencing this pathway because ApoE function can be modified by gender (*19,20*).

In this study, we attempted to clarify this gender discrepancy by measuring brain Aβ plaque load in male and female cohorts of $APP_{swe}/PS1_{\Delta E9}$ mice acutely dosed with bexarotene. We used two different formulations of bexarotene, one in DMSO (as used by Cramer *et al*. (*13*)) and one in corn oil to assess any potential issues with DMSO toxicity. Since RXR and LXR agonists have been shown to modulate microglial activity to dampen their inflammatory responses and enhance their clearance abilities (*21*), we also examined microglial activation in these treated mice. Finally, no study has yet replicated the effect of bexarotene on fear memory, and its cognitive effects remain controversial. Therefore, we evaluated the effect of bexarotene on context-dependent and conditioned-stimulus-dependent fear memory.

Results

To confirm the apparent benefit of acute treatment with bexarotene (13), we initially dosed two cohorts of 8 month old female $APP_{swe}/PS1_{\Delta E9}$ mice with 100 mg/kg of this RXR agonist (or indicated vehicle) by daily oral gavage. We analyzed the effects of treatment on ABCA1 levels in $APP_{swe}/PS1_{\Delta E9}$ mice, and found that the use of DMSO or corn oil as a vehicle does not create a significant difference in the relative means of bexarotene treated groups normalized to their respective vehicle [(M=1.570, SD=0.203)

and (*M*=1.641, *SD*=0.157), respectively F(1,10)=0.044, *p=0.837*], and that there was no interaction between vehicle used and treatment group. As expected, we found that bexarotene significantly increased levels of ABCA1 by 50% after three days of treatment (Fig.1A) [* F(1,13)=5.261, *p=0.027*], confirming that this compound engaged the expected targets in the brains of these mice. To assess the impact of bexarotene on amyloid burden in male and female mice, we dosed an 8 month (DMSO vehicle) and an 11 month old (corn oil vehicle) cohort of $APP_{swe}/PS1_{\Delta E9}$ mice. Again, we found no significant effect of vehicle type on Aβ levels [cortex F(1,29)=0.277, *p=0.965*, hippocampus F(1,29)=3.266, *p=0.081*], and no interaction between vehicle used and treatment group. In contrast to findings of Cramer *et al*. (*13*), no significant differences in Aβ plaque burden were observed in brains of bexarotene treated $APP_{swe}/PS1_{\Delta E9}$ mice compared to vehicle [cortex F(1,29)=0.002, *p=0.965*, hippocampus F(1,29)=0.398, *p=0.533*] (Fig. 1B). Though the sample sizes for each group are small, sample size estimates for each experiment showed that they each have a power ≥88%. In addition, the inability of bexarotene to alter plaque levels in this model has recently been reported by additional groups (*14,15,16,17*). While there has been increasing evidence that plaques may not be as informative correlates of disease as soluble forms of Aβ, the inability of bexarotene to alter soluble Aβ levels in this mouse model has also been recently reported (*14,15,16,17*). Notably, we observed a significant main effect of gender on plaque levels in 11 month old mice. Male groups had significantly lower plaque load compared to female groups [* cortex, F(1,19)=20.177, *p<0.0005* and ** hippocampus F(1,19)=14.045, *p=0.001*] (Fig. 1C). In 8 month old mice, males were not tested, so that

age group could not be included in the analysis for a gender effect, but gender differences in plaque load have been reported as early as six months of age in this mouse model (*18*). Analysis of microglial immunoreactivity using an antisera specific to ionized calcium binding adaptor molecule 1 (Iba1), a microglial inflammatory and phagocytic marker (*22*), revealed a similar pattern between $APP_{swe}/PS1_{\Delta E9}$ mice treated with bexarotene or vehicle (Fig. 2). Despite the potential of RXR agonists to modulate the microglial activation present in $APP_{swe}/PS1_{\Delta E9}$ mice, no significant effect of bexarotene was observed compared with vehicle administration [cortex $F(1,27)=2.231$, $p=0.147$, and hippocampus $F(1,27)=2.127$, $p=0.156$] (Fig. 2A). No significant main effect of gender was found, and no interaction was detected between gender and treatment. Microglial morphology was also analyzed, as described in (*23*). Microglia in transgenic female (Fig. 2B) and male (Fig. 2D) animals show a transitional amoeboid (activating) morphology with clustering of these activated microglia, which was unchanged after administration of bexarotene (Fig. 2C and E, respectively). In contrast, microglia from female and male non-transgenic animals have a uniformly ramified, resting morphology as shown in Additional File 1. A recent study analyzing the presence of Aβ in Iba1-positive microglia also failed to show an effect of bexarotene on Aβ uptake and clearance (*17*).Finally, we analyzed the effects of bexarotene treatment on context-dependent freezing behavior in 8 month old female $APP_{swe}/PS1_{\Delta E9}$ and littermate non-transgenic mice according to the protocol described by Cramer *et al*. (*13*). Behavioral measures in males and females were assessed separately due to gender differences present in this mouse model (*18)*. In the training session, $APP_{swe}/PS1_{\Delta E9}$ receiving vehicle and bexarotene treatment demonstrated similar levels of context-dependent freezing [$F(7,44)=3.905$, $p=0.002$, Tukey: male nontg

p=1.000, male tg *p=0.182*, female nontg, female tg *p=1.000*] (see Fig. 3A) indicating that acquisition of fear response was not significantly affected by genotype, sex, or treatment.

Testing for context-dependent fear memory yielded no significant differences among any of the groups [F(7,44)=1.794, *p=0.113*]. This finding was not surprising given the strong unconditioned stimulus and its multiple presentations in the protocol described in (*13*), which was used here for replication purposes. Of particular note, the group means for context-dependent freezing behavior in Fig. 3A were almost double those reported in Cramer et al. (*13*) using these testing parameters. We also performed a high-sensitivity alternative conditioning paradigm, consisting of a short pre-exposure period and a single delivery of the unconditioned stimulus as described in (*24*) and the Methods. Using this paradigm we detected a significant freezing deficit in 8 month old $APP_{swe}/PS1_{\Delta E9}$ females compared to non-transgenic littermates [F(1,17)=5.943, *p=0.026*] (Fig. 4). However, this deficit was not persistent at 10 months of age [F(1,18)=2.824, *p=0.110*] with an opposing trend of increased freezing in $APP_{swe}/PS1_{\Delta E9}$ females (Fig. 4). These data indicate that freezing behavior might not be robust or reliable measure of cognitive deficits in this mouse model.

We also analyzed conditioned stimulus (CS)-dependent fear responses, and found no effect of bexarotene on freezing behavior in $APP_{swe}/PS1_{\Delta E9}$ mice compared to non-transgenic littermates (Fig. 3B). However, we again observed an unexplained trend of freezing deficit in non-transgenic males treated with bexarotene as compared to vehicle- and bexarotene-treated $APP_{swe}/PS1_{\Delta E9}$ males (Fig 3B). In addition, a significant gender difference was also detected in this task between males and females of vehicle-treated

non-transgenic and $APP_{swe}/PS1_{\Delta E9}$ animals [main effect of gender $F(1,15)=23.506$, $p<0.0005$; main effect of genotype $F(1,15)=1.898$, $p=0.189$, no significant interaction] with females [M=42.006,SD=17.65] showing lower levels of freezing than males [M=76.260,SD=10.50] (Fig. 3B). These gender-related differences were no longer observed in mice treated with bexarotene [males M=48.79, SD=20.71, females M=54.55, SD=21.48; main effect of sex F(1,27)=0.630, $p=0.434$; main effect of genotype F(1,27)=1.388, $p=0.249$; no significant interaction. The condition of equality of variances was not met for this test].

Table 1. Summary of recently published findings on bexarotene in mouse models of Aβ amyloidosis related to the study presented here (first row). N/A indicates that the listed data point was not reported. Superscript numbers indicate reference number of the original work.

Model	Age (months)	Days of Treatment	Brain Insoluble/ Plaque Aβ	Brain Soluble Aβ	Fear Conditioning
$APP_{swe}/PS1_{\Delta E9}$	8 and 11	3, 7, and 14	No effect	N/A	No effect
APP/PS1 + APOE3/4 [14]	7	15	No effect	No effect	N/A
$APP_{swe}/PS1_{\Delta E9}$ [15]	7	11	No effect	No effect	N/A
$APP_{swe}/PS1_{\Delta E9}$ [16]	10	14	No effect	No effect	N/A
$APP_{swe}/PS1_{\Delta E9}$ [17]	6	7	No effect	No effect	N/A
5X FAD [17]	3-4	7	No effect	Decrease Aβ40 only	N/A
APP/PS1-21 [17]	9	26	No effect	No effect	N/A

Discussion

Our data failed to replicate the apparent benefit of acute bexarotene treatment in mouse models of Aβ amyloidosis previously reported (*13*). It is unknown whether chronic administration of bexarotene or alternate dosing strategies would have a beneficial effect. Nevertheless, our failure to replicate the initial observations emphasizes the importance of gender-related differences in the $APP_{swe}/PS1_{\Delta E9}$ mouse model, and other work indicates that these differences may extend to humans (*19,20*). Since the completion of this study, bexarotene has been tested in other animal models of Aβ amyloidosis, including APP/PS1-21 (*17*), 5XFAD (*17*), and $APP_{swe}/PS1_{\Delta E9}$ with APOE3/4 allele knock-in (*14*), as summarized in Table 1. All have failed to replicate a change in soluble or plaque forms of Aβ, with the exception of the non-pathogenic soluble Aβ40 species, which decreased after acute treatment with bexarotene in the 5XFAD mouse model, but not in the $APP_{swe}/PS1_{\Delta E9}$ or the APP/PS1-21 models (*17*).

Importantly, we are unable to replicate a robust and persistent fear conditioning deficit in the $APP_{swe}/PS1_{\Delta E9}$ mouse model, even with an alternate, highly sensitive testing paradigm (*24*). Fear conditioning is the sole behavioral measure previously used to test bexarotene in this model (*13*). In $APP_{swe}/PS1_{\Delta E9}$ mice with APOE3/4 knock-in, bexarotene was reported to rescue deficits in the Radial Arm Water Maze at 7 months of age (*14*), but this testing was also performed on mixed gender cohorts of n=5 per group, introducing a potential false-positive treatment effect. Therefore, the current cognitive preclinical data do not validate the potential of this drug for Alzheimer's therapy.

Together, the array of published work on the effect of bexarotene on pathology and cognitive impairment in mouse models of Aβ amyloidosis produces no rigorous

evidence that bexarotene is a suitable candidate for the treatment of Alzheimer's disease in patients (Table 1). There are potential discrepancies in the formulation of bexarotene used in replicating studies as compared to the original experiments (*13*,*16*) due to lack of availability of this formulation to other research groups. While the consistent upregulation of ABCA1 and ApoE using various formulations of bexarotene (*13,14,15,16,17*) indicates that it does indeed activate the proposed targets, these may not be the true mechanism of action responsible for the changes observed in Cramer *et al*. (*13*). In light of our and other groups (*14,15,16,17*) overall failures to replicate the key findings on bexarotene in mouse models of Aβ amyloidosis, we recommend that the original formulation be made available for rigorous preclinical studies in multiple mouse models in order to clarify the existing discrepancies and to elucidate the mechanism of action before clinical testing progresses.

Methods

Animals. *$APP_{swe}/PS1_{\Delta E9}$* (B6.Cg-Tg(APPswe,PSEN1dE9)85Dbo/Mmjax) were used. 8 month and 11 month old *APPswe/PS1ΔE9* mice were housed on a 14hr dark:10hr light cycle in standard cages with 2-5 mice each and given free access to food and water. Bexarotene (ChemieTek) was dissolved in a vehicle of <15% DMSO in milk or in corn oil, as indicated in the corresponding figure legends. Mice were weighed at the beginning of the treatment period and the necessary volume of solubilized bexarotene was calculated to produce a concentration of 100mg/kg for each animal. Animals were gavaged with vehicle or bexarotene solution daily for 3, 7, or 14 days, as indicated. Studies were performed on mixed gender or females only, where indicated.

Brain ABCA1 quantification. Mice were sacrificed two hours after the day three gavage using brief CO_2 exposure, followed immediately by decapitation. Brains were removed and one hemisphere was collected for ABCA1 quantification. Cortices were quickly dissected on ice with cold forceps. Samples were placed on dry ice in labeled, pre-cooled microfuge tubes. Samples were frozen at -80°C until use. Fresh, cold RIPA buffer (10x volume of sample) with Protease Inhibitor Cocktail was added to samples on ice and tissue was mechanically dissociated using 1mL pipet tips. Samples were sonicated with brief pulses on ice, and centrifuged at 14000rpm for 25 min at 4°C. Supernatants were transferred to new labeled microfuge tubes and kept on ice during protein estimation, or stored at -80°C until use. Protein concentration was estimated using the BCA Assay, and analyzed by the Epoch Com6 spectrophotometer (BioTek) with Gen5 analysis software. Samples for protein blot were prepared containing 1.0-1.5µg protein/µL of sample solution. Samples were mixed, heated at 70°C for five minutes, then cooled and a volume containing 30µg of protein was loaded into wells of 4-12% Bis-Tris gels (Novex) with MOPS running buffer. Gel was run for 120 min at 120 volts, then transferred to a PVDF membrane for 150 min at 30v. Membranes were probed with ABCA1 mouse monoclonal antibody and with antisera against β-tubulin III as a loading control, and were incubated with HRP-conjugated secondary antibodies and exposed to HRP substrate. Exposed films were scanned without any background- or noise-subtraction and analyzed using ImageJ software. The relative optical density of each band was calculated using the area under the curve of lane profile plots on unaltered images. The experiment was replicated in triplicate, and the mean optical density (OD) was calculated.

Aβ Plaque Quantification. Mice were gavaged with 100mg/kg bexarotene for 14 days and sacrificed as described above, and hemispheres were immediately immersed in 4% paraformaldehyde for 24 hours at 4°C. Brains were then moved to PBS solution for 24 hours at 4°C, followed by another change of PBS for storage until use. The tissue was then embedded in paraffin and sectioned into 10μm coronal slices (7B6-stained) or 10μm sagittal slices between 1.2 and 1.5mm from the midline (ubiquitin-stained). Sections were mounted onto slides and stained with ubiquitin (Dako) or 7B6 antibodies (Abcam) to detect Aβ plaques. Plaque area was calculated using the Area Fraction Fractionator probe in the Stereo Investigator stereology program. The counting frame was 150x150 with gridsizes 500x500 μm for cortex and 300x300 μm for hippocampus, and a grid spacing of 10 μm. Plaque area for hippocampus and cortex were measured and normalized to the total area of the brain region for each animal. Data was collected and verified by two independent investigators, blinded to groups.

Iba-1 Quantification and morphological analysis. Animals were sacrificed after 14 days of gavage and their tissues perfused. The brain tissue of each of the animals was removed and placed in a 30% sucrose preservative, and sectioned to a thickness of 40μm on a freezing microtome. Every eighth section was immunostained with anti-Iba1 antibody (1:1000, Wako, cat. #019-19741). Morphology of resting (ramified) and active (amoeboid) microglia was analyzed according to the guidelines specified in (*23*). Briefly, ramified microglia are identified with a small cell body and long, thin projections with distal branching. In contrast, active microglia exhibit a shortening of projections and enlargement of the cell body as they are reabsorbed, leading to an amoeboid morphology.

Fear Conditioning. All mice used for these studies were generated by breeding a single cohort of 10 male and 20 female mice from the line described above. Animals were gavaged with vehicle or bexarotene (100mg/kg) solution daily for 7 days. Behavioral tests were performed in the morning before the daily gavage to minimize any effect of stress from this procedure on behavior. Three days before the start of the test period, animals were handled and the tails marked with permanent marker to eliminate stress caused by checking ear-tags just prior to behavioral testing. The following two days before behavioral testing, each animal was handled and separately habituated to empty waiting cages in a separate room adjacent to the testing room for ten minutes.

Protocol 1:

Context- and Cue-dependent fear conditioning was conducted as described in Cramer et al (*13*), beginning after 4 days of gavage (before the 5th administration). Conditioning was performed in a test chamber with a shock grid floor and a contextual striped and checkered pattern on three of the walls. Testing and data collection were automated by ANY-Maze 4.70 software (Stoelting Co., Wood Dale, IL) according to the following protocol parameters: Light in the chamber 1.5 visible + 1.5 Infrared, Fan ON (65 dB), smell 30% Ethanol, Freezing ON Threshold = 25 msec, Freezing OFF Threshold = 30 msec, Minimum Freezing Duration = 500 msec.

Training Session: Mice were placed in empty waiting cages for ten minutes prior to the start of the test, then placed in the test chamber and allowed to explore for 120 seconds. Mice were then exposed to a conditioned stimulus (CS, 83dB and 2800Hz) for 30 seconds, followed by a 2 second delay, and finally the unconditioned stimulus (US, 0.6 mA) for two seconds. Mice remained in the chamber for an additional 30 seconds to

measure immediate freezing response following the CS/US pairing. This sequence was repeated four times for each animal.

Context dependent freezing: Context-dependent fear behavior was analyzed 24 hours later. Mice were placed in the same test chamber for five minutes without any CS or US administration, and freezing behavior was measured throughout the test.

Conditioned Stimulus (CS)-dependent freezing: An additional 24 hours later, mice were tested for CS-dependent freezing behavior. Mice were placed in a novel test chamber with plain white walls on all sides and a solid floor. Bedding was placed in the bottom of this new chamber, as well as a small paper towel with 1:100 dilution of vanilla extract (McCormick) in water. Mice were allowed to explore the chamber for 120 seconds, followed by CS presentation for 30 seconds, and a 30 second delay to measure immediate freezing response. This sequence was repeated four times for each animal.

Protocol 2:

A high-sensitivity context-dependent fear conditioning protocol (modified from *24*) was also tested in separate cohorts of $APP_{swe}/PS1_{\Delta E9}$ female mice at 5, 8 and 10 months of age. Mice were habituated in the same manner as described previously. The test chamber was identical, with the addition of a scent cue (coconut extract 1:500 in water, McCormick) placed underneath the grid floor. In the Training Session, mice were placed in the test chamber and allowed to explore for 30 seconds. Mice were then exposed to the same unconditioned stimulus as in the previous paradigm (US, 0.6 mA) for two seconds. Mice remained in the chamber for an additional 35 seconds to measure immediate freezing response. 24 hours later, mice were placed in the same test chamber for four minutes without US administration, and time freezing was measured.

Statistical Analysis. Data were analyzed with Univariate Analysis of Variance (ANOVA) using SPSS Statistics 20 software. For Fig. 1, analysis was performed on data in 2x2 (treatment x vehicle or treatment x sex) between-subjects factorial design. For Fig. 2, 3 and 4, analysis was performed in a 2x2 (genotype x sex) between-subjects factorial design for each treatment group, or a 2x2x2 (genotype x sex x treatment) between-subjects factorial design, and main effects and interactions were analyzed. Homogeneity of variance was met for all tests, unless noted otherwise. Significant *p*-value was set to 0.05.

Competing interests

The author(s) declare that they have no competing interests.

Author Contributions Statement

KL and KM performed the primary work on these experiments and wrote the manuscript text. KL prepared the figures. DL assisted in animal gavage and JA in assisted in performing animal surgery, dissections and tissue preparation. AS provided the interpretation of the cognitive testing protocol reported in the original study and prepared all necessary materials and software templates for cognitive testing. AS, JT, and PW provided guidance throughout the project and edited the manuscript.

Acknowledgments

This work is supported by Johns Hopkins ADRC, Alzheimer's Association, Johns Hopkins Brain Science Institute, Johns Hopkins Neuropathology Fund, and a pilot grant from the Memory Disorders Program, Department of Neurology, Georgetown University.

The authors would like to thank V. Nehus, G. Rudow, J. Hussey and B. Zhi for technical support. The ABCA1 antibody was a gift from S. Sisodia (University of Chicago).

Appendix References

[1] Jankowsky JL, Fadale DJ, Anderson J, Xu GM, Gonzales V, Jenkins NA, Copeland NG, Lee MK, Younkin LH, Wagner SL, Younkin SG, Borchelt DR: **Mutant presenilins specifically elevate the levels of the 42 residue beta-amyloid peptide in vivo: evidence for augmentation of a 42-specific gamma secretase**. *Hum Mol Genet*. 2004, **13**(2):159-70.

[2] Burgess BL, McIsaac SA, Naus KE, Chan JY, Tansley GH, Yang J, Miao F, Ross CJ, van Eck M, Hayden MR, van Nostrand W, St George-Hyslop P, Westaway D, Wellington CL: **Elevated plasma triglyceride levels precede amyloid deposition in Alzheimer's disease mouse models with abundant A beta in plasma**. *Neurobiol. Dis*. 2006, **24**(1):114-27.

[3] Wong PC, Savonenko A, Li T, Price DL: **Neurobiology of Alzheimer's Disease**. In: Basic Neurochemistry. Brady, Siegel, Albers and Price (ed.) Eighth Edition, Elsevier Inc., 2012: 815-828.

[4] Jiang Q, Lee CY, Mandrekar S, Wilkinson B, Cramer P, Zelcer N, Mann K, Lamb B, Willson TM, Collins JL, Richardson JC, Smith JD, Comery TA, Riddell D, Holtzman DM, Tontonoz P, Landreth GE: **ApoE promotes the proteolytic degradation of Abeta**. *Neuron* 2008, **58**(5):681-93.

[5] Hashimoto T, Serrano-Pozo A, Hori Y, Adams KW, Takeda S, Banerji AO, Mitani A, Joyner D, Thyssen DH, Bacskai BJ, Frosch MP, Spires-Jones TL, Finn MB, Holtzman

DM, Hyman BT: **Apolipoprotein E, Especially Apolipoprotein E4, Increases the Oligomerization of Amyloid β Peptide**. *J Neurosci*. 2012, **32**(43):15181-92.

[6] Roses AD, Saunders AM: **APOE is a major susceptibility gene for Alzheimer's disease**. *Curr Opin Biotechnol.* 1994, **5**(6):663-667.

[7] Castellano JM, Kim J, Stewart FR, Jiang H, DeMattos RB, Patterson BW, Fagan AM, Morris JC, Mawuenyega KG, Cruchaga C, Goate AM, Bales KR, Paul SM, Bateman RJ, Holtzman DM: **Human ApoE Isoforms Differentially Regulate Brain Amyloid-β Peptide Clearance**. *Sci. Transl. Med*. 2011, **3**(89):89ra57.

[8] Tokuda T, Calero M, Matsubara E, Vidal R, Kumar A, Permanne B, Zlokovic B, Smith JD, LaDu MJ, Rostagno A, Frangione B, and Ghiso J: **Lipidation of apolipoprotein E influences its isoform-specific interaction with Alzheimer's amyloid beta peptides**. *Biochem J*. 2000, **348:**359-65.

[9] Hirsch-Reinshagen V, Zhou S, Burgess BL, Bernier L, McIsaac SA, Chan JY, Tansley GH, Cohn JS, Hayden MR, and Wellington CL: **Deficiency of ABCA1 impairs apolipoprotein E metabolism in brain**. *J Biol Chem*. 2004, **279**:41197–41207.

[10] Wahrle SE, Jiang H, Parsadanian M, Legleiter J, Han X, Fryer JD, Kowalewski T, and Holtzman DM: **ABCA1 is required for normal central nervous system ApoE levels and for lipidation of astrocyte-secreted apoE**. *J Biol Chem*. 2004, **279**:40987–40993.

[11] Bell RD, Sagare AP, Friedman AE, Bedi GS, Holtzman DM, Deane R, and Zlokovic BV: **Transport pathways for clearance of human Alzheimer's amyloid beta-peptide and apolipoproteins E and J in the mouse central nervous system**. *J Cereb Blood Flow Metab*. 2007, **27**:909–918.

[12] Morikawa M, Fryer JD, Sullivan PM, Christopher EA, Wahrle SE, DeMattos RB, O'Dell MA, Fagan AM, Lashuel HA, Walz T, Asai K, Holtzman DM: **Production and characterization of astrocyte-derived human apolipoprotein E isoforms from immortalized astrocytes and their interactions with amyloid-beta**. *Neurobiol Dis*. 2005, **19**:66–76.

[13] Cramer P, Cirroto J, Wesson D, Lee CY, Karlo J, Zinn A, Casali B, Restivo J, Goebel W, James M, Brunden K, Wilson D, Landreth GE: **ApoE-Directed Therapeutics Rapidly Clear β-Amyloid and Reverse Deficits in AD Mouse Models**. *Science* 2012, **23**(335):1503-1506.

[14] Fitz NF, Cronican AA, Lefterov I and Koldamova R: **Comment on "ApoE-directed therapeutics rapidly clear beta-amyloid and reverse deficits in AD mouse models"**. *Science Tech. Comments* 2013: **340**: 924-c.

[15] Price AR, Xu G, Siemienski ZB, Smithson LA, Borchelt DR, Golde TE, Felsenstein KM: : **Comment on "ApoE-directed therapeutics rapidly clear beta-amyloid and reverse deficits in AD mouse models"**. *Science Tech. Comments* 2013, **340**: 924-d.

[16] Tesseur I, Lo AC, Roberfroid A, Dietvorst S, Van Broeck B, Borgers M, Gijsen H, Moechars D, Mercken M, Kemp J, D'Hooge R, De Strooper B. **Comment on "ApoE-directed therapeutics rapidly clear beta-amyloid and reverse deficits in AD mouse models"**. *Science Tech. Comments* 2013, **340**: 924-e.

[17] Veeraraghavalu K, Zhang C, Miller S, Hefendehl JK, Rajapaksha TW, Ulrich J, Jucker M, Holtzman DM, Tanzi RE, Vassar R and Sisodia SS. **Comment on "ApoE-directed therapeutics rapidly clear beta-amyloid and reverse deficits in AD mouse models"**. *Science Tech. Comments* 2013, **340**: 924-f.

[18]Callahan MJ, Lipinski WJ, Bian F, Durham RA, Pack A, and Walker LC: **Augmented senile plaque load in aged female β-amyloid precursor protein – transgenic mice**. *Am. J. Pathol*. 2001, **158**(3):1173-1177.

[19] Kim J, Castellano JM, Jiang H, Basak JM, Parsadanian M, Pham V, Mason SM, Paul SM, Holtzman DM: **Overexpression of low density lipoprotein receptor in the brain markedly inhibits amyloid deposition and increases extracellular A-beta clearance**. *Neuron* 2009, **64**: 632-644.

[20] Damoiseaux JS, Seeley WW, Zhou J, Shirer WR, Coppola G, Karydas A, Rosen HJ, Miller BL, Kramer JH, Greicius MD: **Gender modulates the APOE ε4 effect in healthy older adults: convergent evidence from functional brain connectivity and spinal fluid tau levels**. *J Neurosci*. 2012, **32**(24): 8254-62.

[21] Zelcer N, Khanlou N, Clare R, Jiang W, Reed-Geaghan EG, Landreth GE, Vinters HV, Tontonoz P: **Attenuation of neuroinflammation and Alzheimer's disease pathology by liver x receptors**. *Proc Natl Acad Sci USA* 2007, **104**(25):10601-6.

[22] Ohsawa K, Imai Y, Kanazawa H, Sasaki Y, Kohsaka S: **Involvement of Iba1 in membrane ruffling and phagocytosis of macrophages/microglia**. *J. Cell Sci*. 2000, **113**:3073–3084.

[23] Kettenmann H, Hanisch U-K, Noda M, and Verkhratsky A: **Physiology of Microglia**. *Physiol. Rev*. 2011 **91**(2): 461-553.

[24] McHugh TJ and Tonegawa S: **CA3 NMDA receptors are required for the rapid formation of a salient contextual representation**. *Hippocampus* 2009, **19**: 1153-1158.

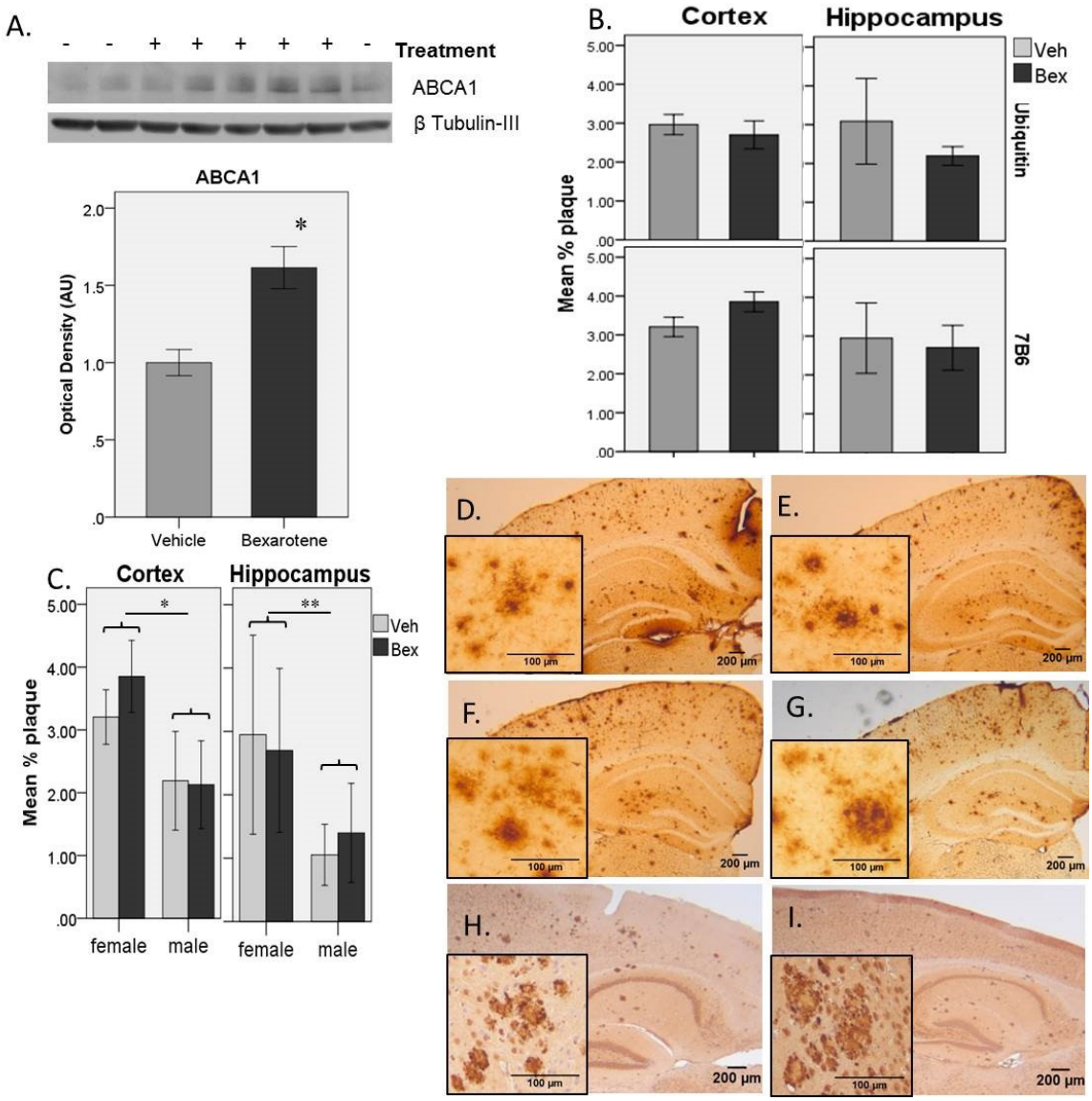

Figure 1. Bexarotene significantly increases ABCA1 in the brains of $APP_{swe}/PS1_{\Delta E9}$ mice, but does not alter Aβ plaques. (A) Representative Western blot (Vehicle (-), Bexarotene (+)) of ABCA1 in cortex of 8.5 mo. female mice, and graph of quantification normalized to β-tubulin-III. Bexarotene significantly increases ABCA1 expression by 50% after three days of gavage treatment [* F(1,13)=5.261, *p=0.027*]. (B) Percent brain area covered by plaques in 8 month (ubiquitin) and 11 month (7B6) female mice, calculated by stereological estimation on sections stained with the antibodies indicated. No significant differences in plaque burden were detected between treatment groups. N-values: Ubiquitin – veh=4, bex=6; 7B6 – veh=3, bex=5. Error bars

represent standard deviation. (C) Gender comparison between % plaque area in 11 mo. mice, calculated by stereological estimation on sections stained with 7B6 antibody. Males had significantly lower plaque load compared to females in both treatment groups [* cortex, F(1,19)=20.177, *p<0.0005* and ** hippocampus F(1,19)=14.045, *p=0.001*]. Error bars represent standard deviation. N-values: females- veh=3, bex5; males- veh=7, bex=8. Sample size estimates show this experiment has power of 88%._Representative images of plaques in $APP_{swe}/PS1_{\Delta E9}$ mice, stained with 7B6 - (D) M Veh (E) M Bex (F) F Veh (G) F Bex - and ubiquitin - (H) F Veh (I) F Bex.

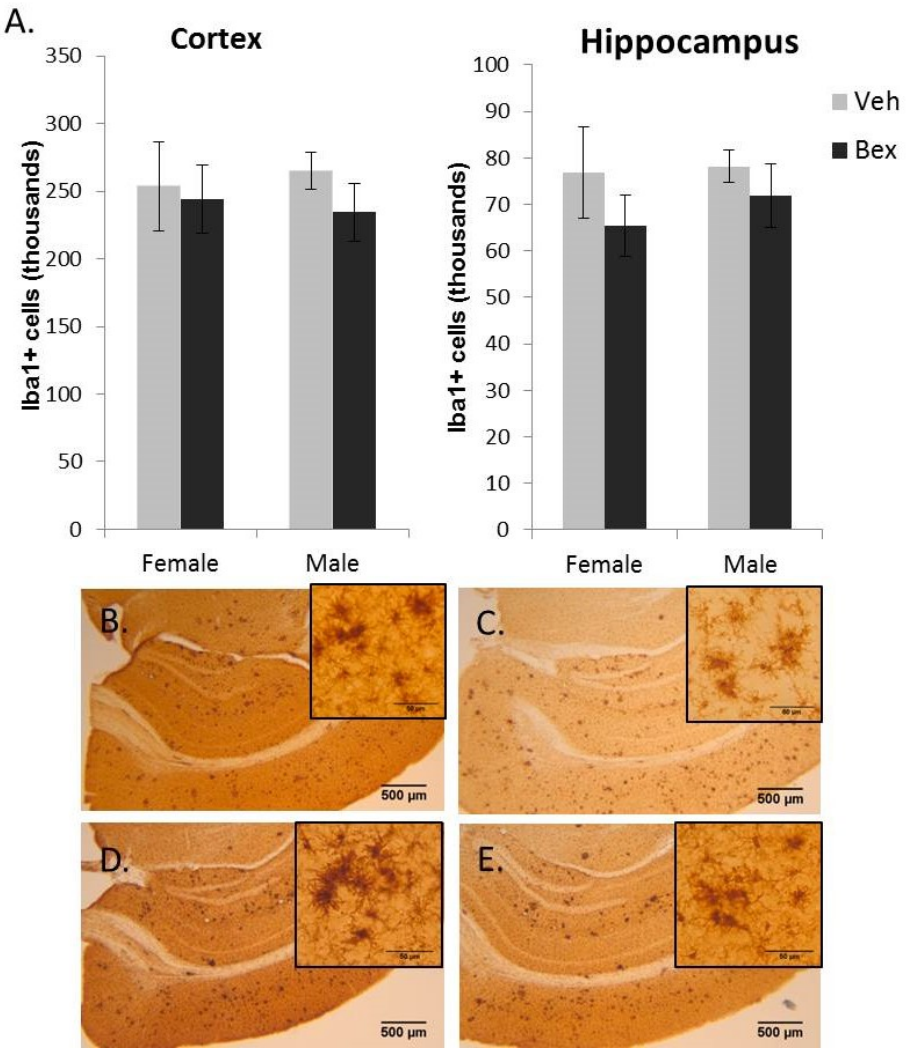

Figure 2. Immunoreactivity of glia is unchanged in $APP_{swe}/PS1_{\Delta E9}$ mice following administration of bexarotene. (A) IBA1 levels in 11 month old male and female $APP_{swe}/PS1_{\Delta E9}$ mice are unaffected by bexarotene treatment in both cortex [F(1,27)=2.231, *p=0.147*] and hippocampus [F(1,27)=2.127, *p=0.156*], and no significant effect of gender was detected [F(1,27)=0.665, *p=0.422*]. No significant interactions were detected. Error bars represent standard deviation. N-values: non-transgenics (veh), males=5, females=5; $APP_{swe}/PS1_{\Delta E9,}$ males: Bex =8, Veh=7, females: Bex=5, Veh=3. Representative images of IBA1 staining and microglial morphology in (B) F tg Veh, (C) F tg Bex, (D) M Tg Veh and (E) M Tg Bex. Scale bars = 500 um large images and 50um on inserts. Morphology shows an amoeboid (active) state with clusters of activated microglia in $APP_{swe}/PS1_{\Delta E9}$ animals (B,D). This morphology and clustering appears unchanged by treatment with bexarotene (C,E).

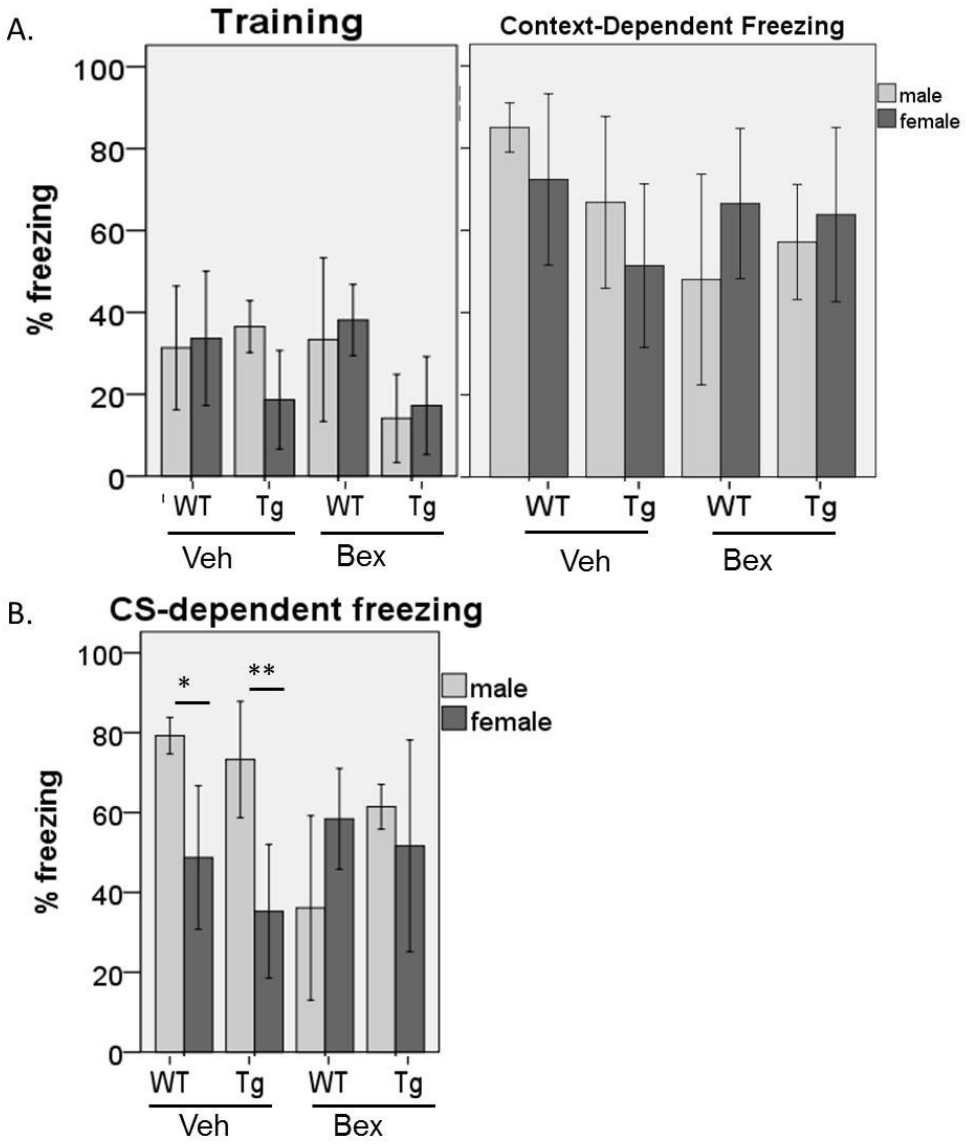

Figure 3. Bexarotene fails to produce an effect on context-dependent or CS-dependent freezing behavior in $APP_{swe}/PS1_{\Delta E9}$ mice. Percent of time spent freezing was measured to quantify long term fear memory. (A) In the training session, $APP_{swe}/PS1_{\Delta E9}$ mice receiving bexarotene treatment demonstrated similar levels of context-dependent freezing compared to their vehicle-treated counterparts [$F(7,44)=3.905$, $p=0.002$; Tukey: male nontg $p=1.000$, male tg $p=0.182$, female nontg $p=0.999$, female tg $p=1.000$]. In the context-dependent testing session, no significant differences were detected among any of the groups [$F(7,44)=1.794$, $p=0.113$]. (B) Analysis of CS-dependent fear responses show no significant effect of bexarotene on freezing behavior in

APP$_{swe}$/PS1$_{ΔE9}$ male or female mice. A significant gender difference was detected between males and females in both non-transgenic and *APP$_{swe}$/PS1$_{ΔE9}$* animals treated with vehicle [main effect of gender $F(1,15)=23.506$, $p<0.0005$; main effect of genotype $F(1,15)=1.898$, $p=0.189$, no significant interaction; females [M=42.006,SD=17.65] show lower levels of freezing than males [M=76.260,SD=10.50]. These gender-related differences were not observed in mice treated with bexarotene [males M=48.79, SD=20.71; females M=54.55, SD=21.48; main effect of sex $F(1,27)=0.630$, $p=0.434$; main effect of genotype $F(1,27)=1.388$,$p=0.249$; no significant interaction]. The condition of equality of variances was not met for this test. For all parts, error bars represent standard deviation. N-values females: nontg-veh=4, AP-veh=7, nontg-bex=8, AP-bex=13. N-values males: nontg-veh=4, AP-veh=4, nontg-bex=6, AP-bex=5.

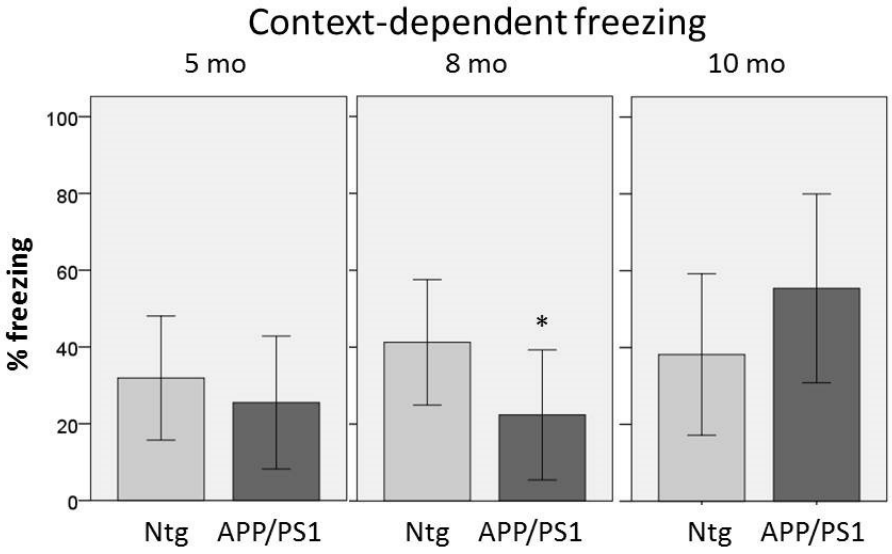

Figure 4. Context-dependent freezing in *APP$_{swe}$/PS1$_{ΔE9}$* female mice and non-transgenic littermates following a high-sensitivity conditioning protocol. A deficit is not yet present in *APP$_{swe}$/PS1$_{ΔE9}$* females at 5 months of age [$F(1,17)=0.684$, $p=0.420$]. Context-dependent freezing deficits are detectable in *APP$_{swe}$/PS1$_{ΔE9}$* females at 8 months of age [*$F(1,17)=5.943$, $p=0.026$], but do not persist to 10 months of age [$F(1,18)=2.824$, $p=0.110$]. N-values: 5 month-nontg=9,

APP/PS1=10, 8 month-nontg=8, APP/PS1=11, 10 month-nontg=12, APP/PS1=8. Error bars represent standard deviation.

Bibliography

1. Barker, W. W. *et al.* Relative frequencies of Alzheimer disease, Lewy body, vascular and frontotemporal dementia, and hippocampal sclerosis in the State of Florida Brain Bank. *Alzheimer Dis. Assoc. Disord.* **16,** 203–12
2. Heron, M. *Deaths: leading causes for 2010. Natl. vital Stat. reports from Centers Dis. Control Prev. Natl. Cent. Heal. Stat. Natl. Vital Stat. Syst.* **62,** (2013).
3. American Psychiatric Association. *Neurocognitive Disorders: Diagnostic and Statistical Manual of Mental Disorders*. (American Psychiatric Publishing, 2013).
4. Arendt, T. Synaptic degeneration in Alzheimer's disease. *Acta Neuropathol.* **118,** 167–179 (2009).
5. Alzheimer's Association. 2016 Alzheimer's Disease Facts and Figures. (2016).
6. Morris, J. C. & Price, J. L. Pathologic Correlates of Nondemented Aging , Mild Cognitive Impairment , and Early-Stage Alzheimer ' s Disease. **17,** 101–118 (2001).
7. Perrin, R. J., Fagan, A. M. & Holtzman, D. M. Multi-modal techniques for diagnosis and prognosis of Alzheimer's disease. *Nature* **461,** 916–922 (2009).
8. Holtzman, D. M., Morris, J. C. & Goate, A. M. Alzheimer's Disease: The Challenge of the Second Century. *Sci. Transl. Med.* **3,** 77sr1 (2011).
9. Musiek, E. S. & Holtzman, D. M. Three dimensions of the amyloid hypothesis: time, space and 'wingmen'. *Nat Neurosci* **18,** 800–806 (2015).
10. Hardy, J. & Higgins, G. Alzheimer's disease: the amyloid cascade hypothesis. *Science (80-.).* **256,** 184–185 (1992).
11. Bekris, L. M., Yu, C.-E., Bird, T. D. & Tsuang, D. W. Genetics of Alzheimer disease. *J. Geriatr. Psychiatry* **23,** 213–227 (2010).
12. Deane, R. *et al.* apoE isoform–specific disruption of amyloid β peptide clearance from mouse brain. *J. Clin. Invest.* **118,** 4002–4013 (2008).
13. Castellano, J. M. *et al.* Human apoE isoforms differentially regulate brain amyloid-β peptide clearance. *Sci. Transl. Med.* **3,** 89ra57 (2011).
14. Corder, A. E. H. *et al.* Gene Dose of Apolipoprotein E Type 4 Allele and the Risk of Alzheimer's Disease in Late Onset Families. *Science (80-.).* **261,** 921–923 (2014).
15. Corder, E. *et al.* Protective effect of apolipoprotein E type 2 allel for late onset Alzheimer disease. *Nat. Genet.* **7,** 180–184 (1994).
16. Ferreira, S. T. & Klein, W. L. The AB oligomer hypothesis for synapse failure and memory loss in Alzheimer's disease. *Neurobiol. Learn. Mem.* **96,** 529–543 (2011).
17. Kim, H. Y. *et al.* EPPS rescues hippocampus-dependent cognitive deficits in APP/PS1 mice by disaggregation of amyloid-β oligomers and plaques. *Nat. Commun.* **6,** 8997 (2015).
18. Vellas, B. *et al.* Long-term follow-up of patients immunized with AN1792: reduced functional decline in antibody responders. *Curr. Alzheimer Res.* **6,** 144–51 (2009).
19. Lemere, C. A. & Masliah, E. Can Alzheimer disease be prevented by amyloid-B immunotherapy? *Nat. Rev. Neurol.* **6,** 108–119 (2010).
20. Morris, G. P., Clark, I. a & Vissel, B. Inconsistencies and controversies

surrounding the amyloid hypothesis of Alzheimer's disease. *Acta Neuropathol. Commun.* **2,** 135 (2014).

21. Herrup, K. The case for rejecting the amyloid cascade hypothesis. *Nat Neurosci* **18,** 794–799 (2015).
22. Holtzman, D. M. *et al.* Apolipoprotein E isoform-dependent amyloid deposition and neuritic degeneration in a mouse model of Alzheimer's disease. *Proc. Natl. Acad. Sci. U. S. A.* **97,** 2892–7 (2000).
23. Lambert, M. P. *et al.* Diffusible, nonfibrillar ligands derived from Abeta1-42 are potent central nervous system neurotoxins. *Proc. Natl. Acad. Sci. U. S. A.* **95,** 6448–53 (1998).
24. Rogaeva, E. *et al.* The neuronal sortilin-related receptor SORL1 is genetically associated with Alzheimer disease. *Nat. Genet.* **39,** 168–77 (2007).
25. Sakae, N. *et al.* ABCA7 Deficiency Accelerates Amyloid-β Generation and Alzheimer's Neuronal Pathology. *J. Neurosci.* **36,** 3848–59 (2016).
26. Reitz, C. Alzheimer's disease and the amyloid cascade hypothesis: A critical review. *Int. J. Alzheimers. Dis.* **2012,** (2012).
27. Kim, J., Basak, J. M. & Holtzman, D. M. The role of apolipoprotein E in Alzheimer's disease. *Neuron* **63,** 287–303 (2009).
28. Hu, F. *et al.* Sortilin-Mediated Endocytosis Determines Levels of the Fronto-Temporal Dementia Protein, Progranulin. *Neuron* **68,** 654–667 (2010).
29. Trougakos, I. P. The molecular chaperone apolipoprotein J/clusterin as a sensor of oxidative stress: implications in therapeutic approaches - a mini-review. *Gerontology* **59,** 514–23 (2013).
30. International Parkinson Disease Genomics Consortium. Imputation of sequence variants for identification of genetic risks for Parkinson's disease: a meta-analysis of genome-wide association studies. - PubMed - NCBI. *Lancet* **377,** 641–9 (2011).
31. Misonou, H., Morishima-Kawashima, M. & Ihara, Y. Oxidative stress induces intracellular accumulation of amyloid beta-protein (Abeta) in human neuroblastoma cells. *Biochemistry* **39,** 6951–9 (2000).
32. Quiroz-Baez, R., Rojas, E. & Arias, C. Oxidative stress promotes JNK-dependent amyloidogenic processing of normally expressed human APP by differential modification of alpha-, beta- and gamma-secretase expression. *Neurochem. Int.* **55,** 662–70 (2009).
33. Leuner, K. *et al.* Mitochondrion-derived reactive oxygen species lead to enhanced amyloid beta formation. *Antioxid. Redox Signal.* **16,** 1421–33 (2012).
34. Liao, Y.-F., Wang, B.-J., Cheng, H.-T., Kuo, L.-H. & Wolfe, M. S. Tumor necrosis factor-alpha, interleukin-1beta, and interferon-gamma stimulate gamma-secretase-mediated cleavage of amyloid precursor protein through a JNK-dependent MAPK pathway. *J. Biol. Chem.* **279,** 49523–32 (2004).
35. O'Meara, E. S. *et al.* Head injury and risk of Alzheimer's disease by apolipoprotein E genotype. *Am. J. Epidemiol.* **146,** 373–84 (1997).
36. Tang, M. X. *et al.* Effect of age, ethnicity, and head injury on the association between APOE genotypes and Alzheimer's disease. *Ann. N. Y. Acad. Sci.* **802,** 6–15 (1996).

37. Jordan, B. D. *et al.* Apolipoprotein E epsilon4 associated with chronic traumatic brain injury in boxing. *JAMA* **278,** 136–40 (1997).
38. Beach, T. G., Monsell, S. E., Phillips, L. E. & Kukull, W. Accuracy of the clinical diagnosis of Alzheimer disease at National Institute on Aging Alzheimer Disease Centers, 2005-2010. *J. Neuropathol. Exp. Neurol.* **71,** 266–73 (2012).
39. Tomiyama, T. *et al.* A new amyloid beta variant favoring oligomerization in Alzheimer's-type dementia. *Ann. Neurol.* **63,** 377–387 (2008).
40. Andrade-Moraes, C. H. *et al.* Cell number changes in Alzheimer's disease relate to dementia, not to plaques and tangles. *Brain* **136,** 3738–52 (2013).
41. Terry, R. D. *et al.* Physical basis of cognitive alterations in Alzheimer's disease: Synapse loss is the major correlate of cognitive impairment. *Ann. Neurol.* **30,** 572–580 (1991).
42. van der Avoort, I. *et al.* Vulvar Squamous Cell Carcinoma. *Int. J. Gynecol. Pathol.* **25,** 22–29 (2006).
43. Nwosu, V., Carpenter, J., Trent, J. M. & Sheridan, R. Heterogeneity of genetic alterations in prostate cancer: evidence of the complex nature of the disease. *Hum. Mol. Genet.* **10,** 2313–2318 (2001).
44. Conteduca, V. *et al.* H. pylori infection and gastric cancer. *Int. J. Oncol.* **42,** 5–18 (2013).
45. Davis, D., Schmitt, F., Wekstein, D. & Markesbery, W. Alzheimer neuropathologic alterations in aged cognitively normal subjects. *J. Neuropathol. Exp. Neurol.* **58,** 376–388 (1999).
46. Rahimi, J. & Kovacs, G. G. Prevalence of mixed pathologies in the aging brain. *Alzheimers. Res. Ther.* **6,** 1–11 (2014).
47. Kovacs, G. G. *et al.* Non-Alzheimer neurodegenerative pathologies and their combinations are more frequent than commonly believed in the elderly brain: a community-based autopsy series. *Acta Neuropathol.* **126,** 365–84 (2013).
48. Neumann, M. *et al.* Ubiquitinated TDP-43 in frontotemporal lobar degeneration and amyotrophic lateral sclerosis. *Science (80-.).* **314,** 130–133 (2006).
49. Stefanis, L. α-Synuclein in Parkinson's disease. *Cold Spring Harb. Perspect. Med.* **2,** a009399 (2012).
50. Probst, A., Tolnay, M., Langui, D., Goedert, M. & Spillantini, M. G. Pick's disease: hyperphosphorylated tau protein segregates to the somatoaxonal compartment. *Acta Neuropathol.* **92,** 588–96 (1996).
51. Amador-Ortiz, C. *et al.* TDP-43 immunoreactivity in hippocampal sclerosis and Alzheimer's disease. *Ann. Neurol.* **61,** 435–45 (2007).
52. Josephs, K. a *et al.* TDP-43 is a key player in the clinical features associated with Alzheimer's disease. *Acta Neuropathol.* **127,** 811–824 (2014).
53. Wang, I.-F., Wu, L.-S., Chang, H.-Y. & Shen, C.-K. J. TDP-43, the signature protein of FTLD-U, is a neuronal activity-responsive factor. *J. Neurochem.* **105,** 797–806 (2008).
54. Liu-Yesucevitz, L. *et al.* Tar DNA binding protein-43 (TDP-43) associates with stress granules: analysis of cultured cells and pathological brain tissue. *PLoS One* **5,** e13250 (2010).

55. Colombrita, C. *et al.* TDP-43 is recruited to stress granules in conditions of oxidative insult. *J. Neurochem.* **111,** 1051–61 (2009).
56. Buratti, E. & Baralle, F. E. Characterization and functional implications of the RNA binding properties of nuclear factor TDP-43, a novel splicing regulator of CFTR exon 9. *J. Biol. Chem.* **276,** 36337–43 (2001).
57. Buratti, E. *et al.* Nuclear factor TDP-43 and SR proteins promote in vitro and in vivo CFTR exon 9 skipping. *EMBO J.* **20,** 1774–84 (2001).
58. Wang, H.-Y., Wang, I.-F., Bose, J. & Shen, C.-K. J. Structural diversity and functional implications of the eukaryotic TDP gene family. *Genomics* **83,** 130–9 (2004).
59. Strong, M. J. *et al.* TDP43 is a human low molecular weight neurofilament (hNFL) mRNA-binding protein. *Mol. Cell. Neurosci.* **35,** 320–7 (2007).
60. Chiang, P.-M. *et al.* Deletion of TDP-43 down-regulates Tbc1d1, a gene linked to obesity, and alters body fat metabolism. *Proc. Natl. Acad. Sci. U. S. A.* **107,** 16320–4 (2010).
61. Polymenidou, M. *et al.* Long pre-mRNA depletion and RNA missplicing contribute to neuronal vulnerability from loss of TDP-43. *Nat. Neurosci.* **14,** 459–468 (2011).
62. Ayala, Y. M. *et al.* TDP-43 regulates its mRNA levels through a negative feedback loop. *EMBO J.* **30,** 277–288 (2011).
63. Shan, X., Chiang, P.-M., Price, D. L. & Wong, P. C. Altered distributions of Gemini of coiled bodies and mitochondria in motor neurons of TDP-43 transgenic mice. *Proc. Natl. Acad. Sci. U. S. A.* **107,** 16325–30 (2010).
64. Burke, K. A., Janke, A. M., Rhine, C. L. & Fawzi, N. L. Residue-by-Residue View of In Vitro FUS Granules that Bind the C-Terminal Domain of RNA Polymerase II. *Mol. Cell* **60,** 231–241 (2015).
65. Molliex, A. *et al.* Phase Separation by Low Complexity Domains Promotes Stress Granule Assembly and Drives Pathological Fibrillization. *Cell* **163,** 123–133 (2015).
66. Jucker, M. & Walker, L. C. Self-propagation of pathogenic protein aggregates in neurodegenerative diseases. *Nature* **501,** 45–51 (2013).
67. Polymenidou, M. & Cleveland, D. W. Prion-like spread of protein aggregates in neurodegeneration. *J. Exp. Med.* **209,** 889–93 (2012).
68. Ling, J. P., Pletnikova, O., Troncoso, J. C. & Wong, P. C. TDP-43 repression of nonconserved cryptic exons is compromised in ALS-FTD. *Science (80-.).* **349,** 650–655 (2015).
69. Sturchler-Pierrat, C. *et al.* Two amyloid precursor protein transgenic mouse models with Alzheimer disease-like pathology. *Proc. Natl. Acad. Sci. U. S. A.* **94,** 13287–92 (1997).
70. Calhoun, M. E. *et al.* Neuron loss in APP transgenic mice. *Nature* **395,** 755–756 (1998).
71. Moechars, D. *et al.* Early phenotypic changes in transgenic mice that overexpress different mutants of amyloid precursor protein in brain. *J. Biol. Chem.* **274,** 6483–92 (1999).

72. Cheng, I. H. *et al.* Aggressive amyloidosis in mice expressing human amyloid peptides with the Arctic mutation. *Nat. Med.* **10,** 1190–2 (2004).
73. Knobloch, M., Konietzko, U., Krebs, D. C. & Nitsch, R. M. Intracellular Abeta and cognitive deficits precede beta-amyloid deposition in transgenic arcAbeta mice. *Neurobiol. Aging* **28,** 1297–306 (2007).
74. Rockenstein, E., Mallory, M., Mante, M., Sisk, A. & Masliaha, E. Early formation of mature amyloid-beta protein deposits in a mutant APP transgenic model depends on levels of Abeta(1-42). *J. Neurosci. Res.* **66,** 573–82 (2001).
75. Games, D. *et al.* Alzheimer-type neuropathology in transgenic mice overexpressing V717F beta-amyloid precursor protein. *Nature* **373,** 523–7 (1995).
76. Lord, A. *et al.* The Arctic Alzheimer mutation facilitates early intraneuronal Abeta aggregation and senile plaque formation in transgenic mice. *Neurobiol. Aging* **27,** 67–77 (2006).
77. Chishti, M. A. *et al.* Early-onset amyloid deposition and cognitive deficits in transgenic mice expressing a double mutant form of amyloid precursor protein 695. *J. Biol. Chem.* **276,** 21562–70 (2001).
78. Davis, J. *et al.* Early-onset and robust cerebral microvascular accumulation of amyloid beta-protein in transgenic mice expressing low levels of a vasculotropic Dutch/Iowa mutant form of amyloid beta-protein precursor. *J. Biol. Chem.* **279,** 20296–306 (2004).
79. Philipson, O. *et al.* A highly insoluble state of Abeta similar to that of Alzheimer's disease brain is found in Arctic APP transgenic mice. *Neurobiol. Aging* **30,** 1393–405 (2009).
80. Herzig, M. C. *et al.* Abeta is targeted to the vasculature in a mouse model of hereditary cerebral hemorrhage with amyloidosis. *Nat. Neurosci.* **7,** 954–60 (2004).
81. Tomiyama, T. *et al.* A mouse model of amyloid beta oligomers: their contribution to synaptic alteration, abnormal tau phosphorylation, glial activation, and neuronal loss in vivo. *J. Neurosci.* **30,** 4845–56 (2010).
82. Kawasumi, M. *et al.* Targeted introduction of V642I mutation in amyloid precursor protein gene causes functional abnormality resembling early stage of Alzheimer's disease in aged mice. *Eur. J. Neurosci.* **19,** 2826–38 (2004).
83. Mucke, L. *et al.* High-level neuronal expression of abeta 1-42 in wild-type human amyloid protein precursor transgenic mice: synaptotoxicity without plaque formation. *J. Neurosci.* **20,** 4050–4058 (2000).
84. Jankowsky, J. L. *et al.* Mutant presenilins specifically elevate the levels of the 42 residue beta-amyloid peptide in vivo: evidence for augmentation of a 42-specific gamma secretase. *Hum. Mol. Genet.* **13,** 159–70 (2004).
85. Garcia-Alloza, M. *et al.* Characterization of amyloid deposition in the APPswe/PS1dE9 mouse model of Alzheimer disease. *Neurobiol. Dis.* **24,** 516–24 (2006).
86. Alonso-Nanclares, L., Merino-Serrais, P., Gonzalez, S. & DeFelipe, J. Synaptic changes in the dentate gyrus of APP/PS1 transgenic mice revealed by electron microscopy. *J. Neuropathol. Exp. Neurol.* **72,** 386–95 (2013).

87. Fernandez-Martos, C. M., King, A. E., Atkinson, R. A. K., Woodhouse, A. & Vickers, J. C. Neurofilament light gene deletion exacerbates amyloid, dystrophic neurite and synaptic pathology in the APP/PS1 transgenic model of Alzheimer's disease. *Neurobiol. Aging* **36,** 2757–2767 (2015).
88. Koffie, R. M. *et al.* Oligomeric amyloid beta associates with postsynaptic densities and correlates with excitatory synapse loss near senile plaques. *Proc. Natl. Acad. Sci. U. S. A.* **106,** 4012–7 (2009).
89. Aso, E. *et al.* Amyloid generation and dysfunctional immunoproteasome activation with disease progression in animal model of familial Alzheimer's disease. *Brain Pathol.* **22,** 636–53 (2012).
90. Pedrós, I. *et al.* Early alterations in energy metabolism in the hippocampus of APPswe/PS1dE9 mouse model of Alzheimer's disease. *Biochim. Biophys. Acta - Mol. Basis Dis.* **1842,** 1556–1566 (2014).
91. Savonenko, A. *et al.* Episodic-like memory deficits in the APPswe/PS1dE9 mouse model of Alzheimer's disease: relationships to beta-amyloid deposition and neurotransmitter abnormalities. *Neurobiol. Dis.* **18,** 602–17 (2005).
92. Zhou, Q. *et al.* Inhibition of c-Jun N-terminal kinase activation reverses Alzheimer disease phenotypes in APPswe/PS1dE9 mice. *Ann. Neurol.* **77,** 637–54 (2015).
93. Iqbal, K., Braak, E., Braak, H., Zaidi, T. & Grundke-Iqbal, I. A silver impregnation method for labeling both Alzheimer paired helical filaments and their polypeptides separated by sodium dodecyl sulfate-polyacrylamide gel electrophoresis. *Neurobiol. Aging* **12,** 357–61 (1991).
94. Duyckaerts, C., Potier, M.-C. & Delatour, B. Alzheimer disease models and human neuropathology: similarities and differences. *Acta Neuropathol.* **115,** 5–38 (2008).
95. Boutajangout, A. *et al.* Increased tau phosphorylation but absence of formation of neurofibrillary tangles in mice double transgenic for human tau and Alzheimer mutant (M146L) presenilin-1. *Neurosci. Lett.* **318,** 29–33 (2002).
96. Hutton, M. *et al.* Association of missense and 5'-splice-site mutations in tau with the inherited dementia FTDP-17. *Nature* **393,** 702–5 (1998).
97. Oddo, S. *et al.* Triple-transgenic model of Alzheimer's Disease with plaques and tangles: Intracellular AB and synaptic dysfunction. *Neuron* **39,** 409–421 (2003).
98. Lewis, J. *et al.* Neurofibrillary tangles, amyotrophy and progressive motor disturbance in mice expressing mutant (P301L) tau protein. *Nat. Genet.* **25,** 402–5 (2000).
99. Umeda, T. *et al.* Neurofibrillary tangle formation by introducing wild-type human tau into APP transgenic mice. *Acta Neuropathol.* **127,** 685–698 (2014).
100. Neary, D. *et al.* Alzheimer's disease: a correlative study. *J. Neurol.* **49,** 229–237 (1986).
101. Scheff, S. W., Price, D. A., Schmitt, F. A. & Mufson, E. J. Hippocampal synaptic loss in early Alzheimer's disease and mild cognitive impairment. *Neurobiol. Aging* **27,** 1372–1384 (2006).
102. Ball, M. J. *et al.* A new definition of Alzheimer's disease: a hippocampal dementia. *Lancet* **1,** 14–16 (1985).

103. Hyman, B. T. & Gomez-Isla, T. Alzheimer's Disease Is a Laminar, Regional, and Neural System Specific Disease, Not A Global Brain Disease. *Neurobiol. Aging* **15,** 353–354 (1994).
104. Gomez-Isla, T. *et al.* Profound Loss of Layer II Entorhinal Cortex Neurons Occurs in Very Mild Alzheimer's Disease. *J. Neurosci.* **16,** 4491–4500 (1996).
105. Josephs, K. A. *et al.* Staging TDP-43 pathology in Alzheimer's disease. *Acta Neuropathol.* **127,** 441–50 (2014).
106. Burgess, B. L. *et al.* Elevated plasma triglyceride levels precede amyloid deposition in Alzheimer's disease mouse models with abundant A beta in plasma. *Neurobiol. Dis.* **24,** 114–27 (2006).
107. LaClair, K. D. *et al.* Treatment with bexarotene, a compound that increases apolipoprotein-E, provides no cognitive benefit in mutant APP/PS1 mice. *Mol. Neurodegener.* **8,** 18 (2013).
108. Workman, A. D., Charvet, C. J., Clancy, B., Darlington, R. B. & Finlay, B. L. Modeling transformations of neurodevelopmental sequences across mammalian species. *J. Neurosci.* **33,** 7368–83 (2013).
109. Kayed, R. *et al.* Fibril specific, conformation dependent antibodies recognize a generic epitope common to amyloid fibrils and fibrillar oligomers that is absent in prefibrillar oligomers. *Mol. Neurodegener.* **2,** 18 (2007).
110. Martin, L., Kaiser, A. & Price, A. Motor neuron degeneration after sciatic nerve avulsion in adult rat evolves with oxidative stress and is apoptosis. *J. Neurobiol.* **40,** 185–201 (1999).
111. Uryu, K. *et al.* Concomitant TAR-DNA-binding protein 43 pathology is present in Alzheimer disease and corticobasal degeneration but not in other tauopathies. *J. Neuropathol. Exp. Neurol.* **67,** 555–64 (2008).
112. Kadokura, A., Yamazaki, T., Lemere, C. a, Takatama, M. & Okamoto, K. Regional distribution of TDP-43 inclusions in Alzheimer disease (AD) brains: their relation to AD common pathology. *Neuropathology* **29,** 566–73 (2009).
113. Xie, H. *et al.* Mitochondrial alterations near amyloid plaques in an Alzheimer's disease mouse model. *J. Neurosci.* **33,** 17042–51 (2013).
114. Shankar, G. M. *et al.* Amyloid-beta protein dimers isolated directly from Alzheimer's brains impair synaptic plasticity and memory. *Nat. Med.* **14,** 837–42 (2008).
115. Zempel, H., Thies, E., Mandelkow, E. & Mandelkow, E.-M. Abeta oligomers cause localized Ca(2+) elevation, missorting of endogenous Tau into dendrites, Tau phosphorylation, and destruction of microtubules and spines. *J. Neurosci.* **30,** 11938–50 (2010).
116. Nixon, R. A. The role of autophagy in neurodegenerative disease. *Nat. Med.* **19,** 983–97 (2013).
117. Chen, D. *et al.* A Mammalian Autophagosome Maturation Mechanism Mediated by TECPR1 and the Atg12-Atg5 Conjugate. *Mol. Cell* **45,** 629–641 (2012).
118. Inoue, K. *et al.* Macroautophagy deficiency mediates age-dependent neurodegeneration through a phospho-tau pathway. *Mol. Neurodegener.* **7,** 48 (2012).

119. Hara, T. *et al.* Suppression of basal autophagy in neural cells causes neurodegenerative disease in mice. *Nature* **441,** 885–9 (2006).
120. Selkoe, D. J. Alzheimer's disease is a synaptic failure. *Science* **298,** 789–791 (2002).
121. Lin, S.-Y. *et al.* GSK3-TIP60-ULK1 signaling pathway links growth factor deprivation to autophagy. *Science* **336,** 477–81 (2012).
122. Small, S. A. & Duff, K. Linking Abeta and tau in late-onset Alzheimer's disease: a dual pathway hypothesis. *Neuron* **60,** 534–42 (2008).
123. Phinney, A. L. *et al.* Cerebral amyloid induces aberrant axonal sprouting and ectopic terminal formation in amyloid precursor protein transgenic mice. *J. Neurosci.* **19,** 8552–8559 (1999).
124. Chin, J. *et al.* Fyn Kinase Modulates Synaptotoxicity , But Not Aberrant Sprouting , in Human Amyloid Precursor Protein Transgenic Mice. *J. Neurosci.* **24,** 4692–4697 (2004).
125. Rosenblum, W. I. Why Alzheimer trials fail: Removing soluble oligomeric beta amyloid is essential, inconsistent, and difficult. *Neurobiol. Aging* **35,** 969–974 (2014).
126. de Flores, R., La Joie, R. & Chetelat, G. Structural imaging of hippocampal subfields in healthy aging and Alzheimer's disease. *Neuroscience* **309,** 29–50 (2015).
127. Sevigny, J. & Neurimmune. Biogen IDEC presents positive interim results from Phase 1b study. in *12th Int. Conf. Alzheimer's Park. Dis. Relat. Neurol. Disord.* (2015).
128. Henley, D. B., Sundell, K. L., Sethuraman, G., Dowsett, S. a & May, P. C. Safety profile of semagacestat, a gamma-secretase inhibitor: IDENTITY trial findings. *Curr. Med. Res. Opin.* **7995,** 1–12 (2014).
129. Li, T., Ma, G., Cai, H., Price, D. L. & Wong, P. C. Nicastrin is required for assembly of presenilin/gamma-secretase complexes to mediate Notch signaling and for processing and trafficking of beta-amyloid precursor protein in mammals. *J. Neurosci.* **23,** 3272–7 (2003).
130. Saura, C. A. *et al.* Loss of presenilin function causes impairments of memory and synaptic plasticity followed by age-dependent neurodegeneration. *Neuron* **42,** 23–36 (2004).
131. Bammens, L., Chávez-Gutiérrez, L., Tolia, A., Zwijsen, A. & De Strooper, B. Functional and topological analysis of Pen-2, the fourth subunit of the gamma-secretase complex. *J. Biol. Chem.* **286,** 12271–82 (2011).
132. Chávez-Gutiérrez, L. *et al.* The mechanism of γ-Secretase dysfunction in familial Alzheimer disease. *EMBO J.* **31,** 2261–74 (2012).
133. Veeraraghavalu, K. *et al.* Comment on 'ApoE-directed therapeutics rapidly clear β-amyloid and reverse deficits in AD mouse models'. *Science* **340,** 924–f (2013).
134. Fitz, N. F., Cronican, A. A., Lefterov, I. & Koldamova, R. Comment on: ApoE-directed therapeutics rapidly clear β- amyloid and reverse deficits in AD mouse models. *Science (80-.).* **340,** 924–92c (2013).
135. Price, A. R., Xu, G., Siemienski, Z. B., Smithson, L. A. & Borchelt, D. R.

Comment on ‘ApoE-directed therapeutics rapidly clear β-amyloid and reverse deficits in AD mouse models’. *Science (80-.).* **340,** 924–d (2013).

136. Tesseur, I. *et al.* Comment on ‘ApoE-directed therapeutics rapidly clear β-amyloid and reverse deficits in AD mouse models’. *Science (80-.).* **340,** 924 (2003).
137. Cramer, P. E. *et al.* ApoE-directed therapeutics rapidly clear β-amyloid and reverse deficits in AD mouse models. *Science* **335,** 1503–6 (2012).
138. De Strooper, B. Lessons from a failed gamma-secretase Alzheimer trial. *Cell* **159,** 721–726 (2014).

CURRICULUM VITAE

The Johns Hopkins University School of Medicine

Katherine D. LaClair, B.A. 6/1/2016

Born Dec. 1, 1988, New York, NY, USA

Educational History

Ph.D.	2016	Cellular and Molecular Medicine Program Mentor: Philip C. Wong, Ph.D.	Johns Hopkins SOM
B.A.	2010	Specialized Honors in Neuroscience Mentor: Roger B. Knowles Ph.D.	Drew University

Other Research Experience

Undergraduate Research Fellow, 2008-2010 Lab of Dr. Roger Knowles, Drew University

Summer Undergrad. Research Fellow, 2009 Lab of Dr. Sidney Strickland, The Rockefeller University

Selected Honors and Awards

Pathology Young Investigator's Day Award for Excellence in Translational Research 2015, JHUSOM

Graduation with Specialized Honors, *summa cum laude* 2010, Drew University

Novartis Science Scholarship 2008-2010, Novartis Pharmaceuticals

Honorable Mention, Barry M. Goldwater Memorial Scholarship 2009, United States Congress

Tracy J. Shors Prize in Neuroscience 2009, Drew University

Publications

Peer-reviewed original research articles

LaClair KD, Manaye KF, Lee DL, Allard JS, Savonenko AV, Troncoso JC, Wong PC. 2013. Treatment with bexarotene, a compound that increases apolipoprotein-E, provides no cognitive benefit in mutant APP/PS1 mice. *Mol Neurodegener*. 8(1):18. PMCID: PMC3693923.

Abstracts

Bell WR, Sun M, **LaClair KD**, Ling JP, Pletnikova O, Troncoso JC, Wong PC, Chen L. June 2016. Impaired TDP-43 Repression of Non-conserved Cryptic Exons in Alzheimer's Disease. *American Association of Neuropathologists*, Baltimore, MD.

Pletnikova O, Rudow GL, Kageyama Y, **LaClair KD**, Fowler D, Martin LJ, Troncoso JC. June 2016. The spectrum of preclinical Alzheimer's pathology and its modulation by ApoE genotype. *American Association of Neuropathologists*, Baltimore, MD.

LaClair KD, Wong PC. October 2015. Determining the role of TDP-43 in Alzheimer's disease-related neurodegeneration. Program # 487.19/D2, *Society for Neuroscience*, Chicago, IL.

LaClair KD, Wong PC. March 2015. Determining the Role of TDP-43 in Alzheimer's disease. *Presented at 17th Annual Young Investigator's Day*, Department of Pathology, JHUSOM, Baltimore, MD.

LaClair KD, Petrack B, and Knowles RB. 2010. Analysis of Mitochondrial Dynamics in a Cell Culture Model of Alzheimer's disease and Evaluation of the Mechanism of Action of Methylene Blue as a Potential Treatment. Poster Presentation, *The 38th Annual Hunter College Psychology Convention & The 14th Annual N.E.U.R.O.N. Conference*, New York City, NY.

Service and Leadership

Chair of Ethical Action Committee, 2012-2015 Baltimore Ethical Society, Baltimore MD

Co-mentor to rotation Ph.D. student, 2013 Laboratory of Dr. Philip C. Wong, JHUSOM

Teaching Assistant, "Scientific Foundations of Medicine" course , 2013 JHUSOM

Co-mentor to undergraduate student, 2012 Lab of Dr. Philip C. Wong, JHUSOM

Teaching Assistant "Great Challenges in Neuroscience" course, 2010 Lab of Dr. Roger B. Knowles, Drew University

Teaching Assistant, "Cell and Molecular Neurobiology Lab", 2009 Drew University